Formulating the Equations of Ocean Models

Stephen M. Griffies

*National Oceanic and Atmospheric Administration (NOAA) Geophysical Fluid Dynamics Laboratory,
Princeton, New Jersey, USA*

Alistair J. Adcroft

*Princeton University Atmospheric and Oceanic Sciences Program,
Princeton, New Jersey, USA*

We formulate mathematical equations describing the thermo-hydrodynamics of
the ocean and introduce certain numerical methods employed by models used for
ocean simulations.

1. INTRODUCTION

The purpose of this chapter is to formulate the equations of ocean models and to outline solution methods. Global ocean climate models, including those representing mesoscale eddies, are traditionally based on the hydrostatic primitive equations. We nonetheless discuss extensions to the more fundamental non-hydrostatic equations, which are used in certain fine resolution process studies, such as for convection and mixing, and increasingly for coastal and regional modeling. The target audience for this chapter includes students and researchers interested in fundamental physical and numerical aspects of ocean models. We thus aim to present a reasonably concise yet thorough accounting of the rationalization required to pose the problem of ocean modeling. We take a first principles perspective to allow readers with little background in ocean fluid mechanics to follow the full development. This goal necessitates starting from the basics as we develop the model equations and methods. For this purpose, much material was culled from various research papers and textbooks, such as *Gill* [1982], *Pedlosky* [1987], *Lion et al*. [1992], *Marshall et al*. [1997], *Haidvogel and Beck-*

mann [1999], *Griffies et al*. [2000a], *Griffies* [2004, 2005], *Vallis* [2006], *Higdon* [2006], and *Müller* [2006].

Our presentation focuses on developing the fluid mechanics of the ocean and weaves into this discussion elements appropriate for the formulation of ocean models. We begin with a discussion of ocean fluid kinematics in Section 2 where we introduce mass conservation as well as the notions of dia-surface transport. Section 3 then focuses on tracer budgets, which follow quite naturally from mass budgets, only with the introduction of possible nontrivial fluxes of tracer which occur in the absence of mass fluxes. Section 4 introduces a dynamical description that arises from the use of Newton's Second Law of Motion applied to continuous fluid parcels. Section 5 presents the equation of state for density and discusses the material evolution of density. Section 6 derives some energetic properties of the equations of motion, with energetics providing a guiding principle for developing certain numerical solution methods. Section 7 introduces notions of non-equilibrium thermodynamics, a subject which forms the basis for establishing budgets of heat within the ocean. Section 8 linearizes the dynamical equations to deduce various linear modes of motion fundamental to ocean dynamics. These motions also have direct relevance to the development of methods used to solve the ocean equations. They furthermore motivate certain approximations or filters used to simplify the supported dynamical modes, with certain approximations described in Section 9. Section 10 presents an overview of vertical coordinates. The

choice of vertical coordinate is fundamental to the numerical algorithms of an ocean model. Section 11 presents a general discussion of solution methods used for numerical models of the ocean. Section 12 closes this chapter with a brief summary and discussion of certain features of ocean modeling that present a barrier between what is desired theoretically and what is realizable in practice.

2. KINEMATICS

Kinematics is the study of intrinsic properties of motion without concern for dynamical laws. Fluid kinematics is concerned with establishing constraints on fluid motion due to interactions with geometrical boundaries of the domain, such as the land–sea, ice–sea, and air–sea boundaries of an ocean basin. A fundamental element of kinematics is the set of coordinates used to describe motion. For fluid motion, we are led to notions of generalized vertical coordinates, which are a critical element in theoretical and numerical models of the ocean. Although not strictly a kinematic issue, fluid kinematics also concerns itself with establishing the balances of mass for infinitesimal fluid parcels, as well as for finite regions.

It is convenient and conventional to formulate the mechanics of a continuous fluid by focusing on infinitesimal mass conserving parcels [e.g., *Batchelor*, 1967]. Choosing to do so allows many notions from classical particle mechanics to transfer over to continuum mechanics of fluids, especially when describing fluid motion from a Lagrangian perspective. Mass conservation is also a fundamental property of the ocean, with the mass of the ocean changing only through boundary input.

2.1. Parcel Kinematics

Consider an infinitesimal parcel of seawater contained in a volume $dV = dx\,dy\,dz$ with a mass $dM = \rho\,dV$, where ρ is the in situ mass density of the parcel and $\mathbf{x} = (x, y, z)$ is the Cartesian coordinate of the parcel with respect to an arbitrary origin. Conservation of mass for this parcel implies that dM is materially constant, i.e., $d/dt\,(dM) = 0$. For convenience, we write mass conservation as

$$\frac{d}{dt}\ln(dM) = 0. \tag{1}$$

Mass conservation is realized as the parcel volume and density change in complementary manners where the volume of a fluid parcel changes according to the divergence of the velocity field

$$\frac{d}{dt}\ln(dV) = \nabla \cdot \mathbf{v}, \tag{2}$$

and the density changes according to the convergence

$$\frac{d}{dt}(\ln\rho) = -\nabla \cdot \mathbf{v}. \tag{3}$$

Hence, parcel volume increases when moving through a diverging velocity field, while the density decreases.

The mass budget, given equivalently by equations (1)–(3), describes fluid motion from the perspective of a moving fluid parcel. This perspective provides a Lagrangian description of fluid motion. The complementary Eulerian perspective measures fluid properties from a fixed-space frame. Time tendencies in the two reference frames are related by the coordinate transformation

$$\frac{d}{dt} = \partial_t + \mathbf{v} \cdot \nabla, \tag{4}$$

where ∂_t measures Eulerian time tendencies from a fixed-space point. The advection term $\mathbf{v}\cdot\nabla$ reveals the fundamentally nonlinear character of fluid dynamics, with the parcel's velocity $\mathbf{v} = d\mathbf{x}/dt$ measuring the time changes of its position.[1] Use of relation (4) converts the Lagrangian statement of mass conservation given by equation (1) to the Eulerian form

$$\rho_{,t} + \nabla \cdot (\rho\,\mathbf{v}) = 0. \tag{5}$$

This equation is termed the mass continuity equation. Note that we introduced a comma as shorthand for the partial time derivative taken at a fixed point in space

$$\rho_{,t} = \partial\rho/\partial t. \tag{6}$$

We use an analogous notation for other partial derivatives.[2] A useful relation used throughout this chapter follows by combining the material time derivative in equation (4) with mass continuity in equation (5) to render

$$\rho\frac{d\Psi}{dt} = (\rho\,\Psi)_{,t} + \nabla \cdot (\rho\,\mathbf{v}\,\Psi), \tag{7}$$

where Ψ is any scalar field.

It is common in fluid mechanics to move between the Lagrangian and Eulerian descriptions, as they offer useful complementary insights. Certain ocean models likewise exploit the advantages of these two descriptions. For example, the vertical coordinate in isopycnal models moves with the motions of an adiabatic fluid parcel. It is therefore a Lagrangian vertical coordinate. In contrast, geopotential vertical coordinate models retain a fixed vertical position as determined by the static depth of a grid cell, and so this is an Eulerian vertical coordinate. Horizontal coordinates in most ocean models remain fixed in space, and so are Eulerian.

2.2. Dia-Surface Transport

In providing a mechanistic description of ocean budgets, it is often useful to measure the material or momentum transfer through a surface. This transport is termed the dia-surface transport. We are particularly interested in the transport through three surfaces, with the following general discussion relevant for each.

The first surface is the ocean free surface. Here, water and tracer penetrate this surface through precipitation, evaporation, river runoff (when applied as an upper ocean boundary condition), and sea ice melt. Momentum exchange arises from stresses between the ocean and atmosphere or ice. The ocean free surface can be represented mathematically by the identity $z - \eta(x, y, t) = 0$. For mathematical expediency, we assume that the surface height η is smooth and contains no overturns at the scales of interest. That is, we assume that breaking surface waves are filtered or averaged.

Second, we may describe the solid Earth lower boundary mathematically by using the time-independent expression $z + H(x, y,) = 0$. It is typically assumed that there is no fluid mass transport through the solid Earth. However, in the case of geothermal heating, we may consider an exchange of heat between the ocean and the solid Earth. Momentum exchange through the action of stresses occur between the solid Earth and ocean fluid.

Third, within the ocean interior, transport across surfaces of constant generalized vertical coordinate $s = s(x, y, z, t)$ constitutes the dia-surface transport affecting budgets of mass, tracer, and momentum within layers bounded by two generalized vertical coordinate surfaces. A canonical example is provided by isopycnal layers formed by surfaces of constant potential density, as used in isopycnal ocean models as well as theoretical descriptions of adiabatic ocean dynamics. A surface of constant generalized vertical coordinate can be successfully used to partition the vertical so long as the transformation between the generalized vertical coordinate and the geopotential is invertible. The Jacobian of transformation is given by $z_{,s}$, which must then be single signed for useful vertical coordinates. This constraint means that we do not allow the surfaces to overturn, which is the same assumption made about the ocean surface $z = \eta(x, y, t)$. This restriction places a limitation on the ability of isopycnal models to describe non-hydrostatic processes, such as overturning, common in Kelvin–Helmholz billows or vertical convection. We refer to the Jacobian $z_{,s}$ as the specific thickness, with this name motivated by noting that the vertical thickness of a layer of coordinate thickness ds is given by d$z = z_{,s}$ ds.

To develop the mathematical description of dia-surface fluid transport, we note that at an arbitrary point on a surface
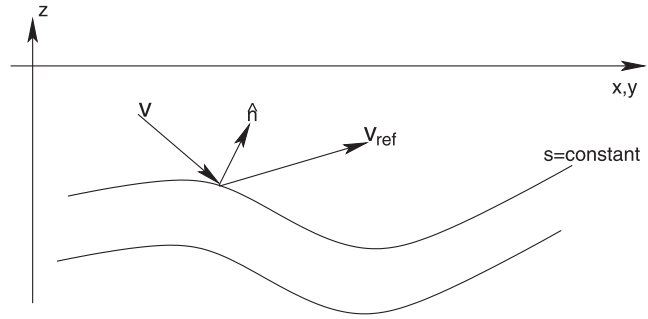

Figure 1. Surfaces of constant generalized vertical coordinate living interior to the ocean. An upward normal direction $\hat{\mathbf{n}}$ is indicated on one of the surfaces. Also shown is the orientation of the velocity of a fluid parcel $\mathbf{v}$ and the velocity $\mathbf{v}^{(\text{ref})}$ of a reference point living on the surface.

of constant generalized vertical coordinate (see Figure 1), the rate at which fluid moves in the direction normal to the surface is given by

$$\text{rate of flow in direction } \hat{\mathbf{n}} = \mathbf{v} \cdot \hat{\mathbf{n}}. \tag{8}$$

In this equation, $\hat{\mathbf{n}} = \nabla s |\nabla s|^{-1}$ is the surface unit normal direction. If we are working with the free surface, then the unit normal takes the form $\hat{\mathbf{n}} = \nabla(z - \eta)/|\nabla(z - \eta)|$, whereas at the solid Earth bottom, $\hat{\mathbf{n}} = -\nabla(z + H)/|\nabla(z + H)|$. Introducing the material time derivative ds/d$t = s_{,t} + \mathbf{v} \cdot \nabla s$ to equation (8) leads to the equivalent expression

$$\mathbf{v} \cdot \hat{\mathbf{n}} = |\nabla s|^{-1}(\mathrm{d}/\mathrm{d}t - \partial_t)s. \tag{9}$$

That is, the normal component to the velocity of a fluid parcel is proportional to the difference between the material time derivative of the surface and its partial time derivative.

As the surface is generally moving (except the solid Earth lower boundary), the net flux of seawater penetrating the surface is obtained by subtracting the velocity of the surface $\mathbf{v}^{(\text{ref})}$ in the $\hat{\mathbf{n}}$ direction from the velocity component $\mathbf{v} \cdot \hat{\mathbf{n}}$ of the fluid parcels

$$\begin{aligned}\text{rate of relative normal flow} \\ \text{across surface} = \hat{\mathbf{n}} \cdot (\mathbf{v} - \mathbf{v}^{(\mathbf{ref})}).\end{aligned} \tag{10}$$

The velocity $\mathbf{v}^{(\text{ref})} = \mathbf{u}^{(\text{ref})} + w^{(\text{ref})} \hat{\mathbf{z}}$ is that of a reference point fixed on the surface. Correspondingly, the material time derivative of the surface, taken with respect to the reference velocity, vanishes: $\mathrm{d}^{(\text{ref})} s/\mathrm{d}t = 0$. This result allows us to write the reference vertical velocity component $w^{(\text{ref})} = \mathrm{d}z^{(\text{ref})}/\mathrm{d}t$ as $w^{(\text{ref})} = -z_{,s}(\partial_t + \mathbf{u}^{(\text{ref})} \cdot \nabla_z)s$, thus rendering

$$\hat{\mathbf{n}} \cdot \mathbf{v}^{(\mathrm{ref})} = -s_{,t} \, |\nabla s|^{-1}. \tag{11}$$

Hence, the normal component to the velocity of the surface vanishes when the surface is static, as may be expected. When interpreting the dia-surface velocity component below, we find it useful to note that relation (11) leads to

$$z_{,s} \nabla s \cdot \mathbf{v}^{(\mathrm{ref})} = z_{,t}. \tag{12}$$

To reach this result, we used the identity $s_{,t}\, z_{,s} = -z_{,t}$, with $z_{,t}$ the time tendency for the depth of a particular constant s surface.

Using expression (11) in equation (10) for the net flux of seawater crossing the surface leads to

$$\hat{\mathbf{n}} \cdot (\mathbf{v} - \mathbf{v}^{(\mathrm{ref})}) = |\nabla s|^{-1} \mathrm{d}s/\mathrm{d}t. \tag{13}$$

The material time derivative of the generalized surface thus vanishes if and only if no water parcels cross it. This is a very important result that is used throughout ocean theory and modeling. It provides an expression for the volume of seawater crossing a generalized surface, per time, per area. The area normalizing the volume flux is that area $\mathrm{d}A_{(\hat{\mathbf{n}})}$ of an infinitesimal patch on the surface of constant generalized vertical coordinate with outward unit normal $\hat{\mathbf{n}}$. This area can generally be written $\mathrm{d}A_{(\hat{\mathbf{n}})} = |z_{,s} \nabla s| \mathrm{d}A$, where $\mathrm{d}A = \mathrm{d}x\mathrm{d}y$ is the area of the surface projected onto the horizontal plane formed by surfaces of constant depth. Hence, the volume per time of fluid passing through the generalized surface $\hat{\mathbf{n}} \cdot (\mathbf{v} - \mathbf{v}^{(\mathrm{ref})}) \mathrm{d}A_{(\hat{\mathbf{n}})}$ is equivalent to $|z_{,s}|(\mathrm{d}s/\mathrm{d}t)\mathrm{d}A$. This result motivates us to introduce the dia-surface velocity component

$$w^{(s)} = z_{,s} \frac{\mathrm{d}s}{\mathrm{d}t}, \tag{14}$$

which measures the volume of fluid passing through the surface, per unit horizontal area, per unit time. That is,

$$w^{(s)} \equiv \frac{\hat{\mathbf{n}} \cdot (\mathbf{v} - \mathbf{v}^{(\mathrm{ref})}) \, \mathrm{d}A_{(\hat{\mathbf{n}})}}{\mathrm{d}A} \tag{15}$$

$$= \frac{(\text{volume/time})\text{fluid through surface}}{\text{horizontal area of surface}}. \tag{16}$$

The dia-surface velocity component can be written in the following equivalent forms

$$w^{(s)} = z_{,s} \, \mathrm{d}s/\mathrm{d}t$$

$$= z_{,s} \nabla s \cdot (\mathbf{v} - \mathbf{v}^{(\mathrm{ref})})$$

$$= (\hat{\mathbf{z}} - \nabla_s z) \cdot \mathbf{v} - z_{,t}$$

$$= w - (\partial_t + \mathbf{u} \cdot \nabla_s) z \tag{17-20}$$

where $\nabla_s z = -z_{,s} \nabla_z s$ is the slope of the s surface projected onto the horizontal directions, and the penultimate step follows from the identity (12). When the surface is static, then the dia-surface velocity component reduces to $w^{(s)} = w - \mathbf{u} \cdot \nabla_s z$. If the surface is flat, then the dia-surface velocity component measures the flux of fluid moving vertically relative to the motion of the generalized surface. Finally, if the surface is flat and static, the dia-surface velocity component becomes the vertical velocity component $w = \mathrm{d}z/\mathrm{d}t$ used in geopotential coordinate models.

The expression (14) for $w^{(s)}$ brings the material time derivative (4) into the following equivalent forms

$$\frac{\mathrm{d}}{\mathrm{d}t} = \left(\frac{\partial}{\partial t}\right)_z + \mathbf{u} \cdot \nabla_z + w \left(\frac{\partial}{\partial t}\right) \tag{21}$$

$$= \left(\frac{\partial}{\partial t}\right)_s + \mathbf{u} \cdot \nabla_s + \frac{\mathrm{d}s}{\mathrm{d}t}\left(\frac{\partial}{\partial s}\right) \tag{22}$$

$$= \left(\frac{\partial}{\partial t}\right)_s + \mathbf{u} \cdot \nabla_s + w^{(s)}\left(\frac{\partial}{\partial z}\right), \tag{23}$$

where $\partial_s = z_{,s}\, \partial_z$ provides a relationship between the vertical coordinate partial derivatives. Note that the subscripts in these expressions denote variables held fixed for the partial derivatives. We highlight the special case of no fluid parcels crossing the generalized surface. This occurs in the case of adiabatic flows with $s = \rho$ being an isopycnal coordinate. For adiabatic flow, the material time derivative in equation (23) only has a horizontal two-dimensional advective component $\mathbf{u} \cdot \nabla_\rho$. This result should not be interpreted to mean that the velocity of a fluid parcel in an adiabatic flow is strictly horizontal. Indeed, it generally is not, as the form given by equation (21) makes clear. Rather, it means that the advective transport of fluid properties occurs along surfaces of constant ρ, and such transport is measured by the convergence of horizontal advective fluxes as measured along surfaces of constant ρ.

2.3. Kinematic Boundary Conditions

The discussion so far of dia-surface transport focused on a surface with a constant generalized vertical coordinate within the ocean interior. These results can also be applied to the ocean free surface (Figure 2) and solid Earth lower boundary to derive kinematic boundary conditions. For the lower boundary, again assuming no material transport through the boundary, we have the trivial result

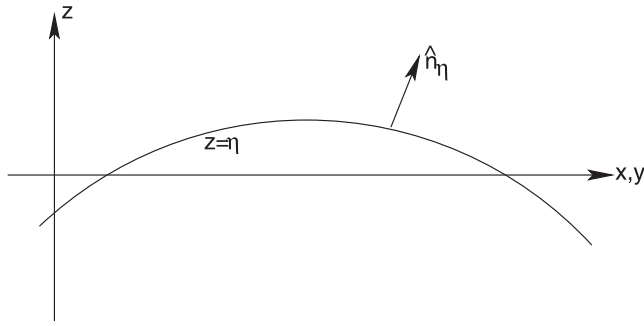$$w^{(s)} = 0 \quad \text{at} \ s = s_{\mathrm{bot}}, \tag{24}$$

$$\rho \left(\frac{\mathrm{d}(z - \eta)}{\mathrm{d}t} \right) = -\rho_{\mathrm{w}} q_{\mathrm{w}} \qquad \text{at } z = \eta. \qquad (28)$$

The identity $\mathrm{d}z/\mathrm{d}t = z_{,s} \, \mathrm{d}s/\mathrm{d}t$ leads to the kinematic boundary condition in generalized vertical coordinates

$$\rho \, z_{,s} \left(\frac{\mathrm{d}(s - s_{\mathrm{top}})}{\mathrm{d}t} \right) = -\rho_{\mathrm{w}} q_{\mathrm{w}} \qquad \text{at } s = s_{\mathrm{top}}, \qquad (29)$$

where $s_{\mathrm{top}} = s(x, y, z = \eta, t)$ is the value of the generalized vertical coordinate at the ocean surface.

These material statements of the kinematic boundary condition can also be derived by considering the mass budget over either an infinitesimal region near the upper ocean surface, or the budget over a full column of water extending from a static ocean bottom at $z = -H(x, y)$ to a dynamic ocean surface at $z = \eta(x, y, t)$. We present the column mass budget approach because it has application for later considerations. The total mass per horizontal area of fluid inside the column is given by the integral $\int_{-H}^{\eta} \rho \, \mathrm{d}z$. Conservation of mass for this column implies that mass changes in time through imbalances in fluxes crossing the ocean free surface and convergence of advective mass transport through the vertical sides of the column.[4] These considerations lead to the balance

$$\partial_t \left(\int_{-H}^{\eta} \mathrm{d}z \, \rho \right) + \nabla \cdot \mathbf{U}^\rho = q_{\mathrm{w}} \rho_{\mathrm{w}}, \qquad (30)$$

where

$$\mathbf{U}^\rho = \int_{-H}^{\eta} \mathrm{d}z \, \rho \, \mathbf{u} \qquad (31)$$

is a shorthand notation for the vertically integrated horizontal momentum per volume. Now, to derive the surface kinematic boundary condition, perform the derivative operations on the integrals in the mass budget expressed in equation (30), use the no-flux lower boundary condition, and use the Eulerian mass conservation relation (5) to render

$$\rho \, (\partial_t + \mathbf{u} \cdot \nabla) \, \eta = \rho_{\mathrm{w}} q_{\mathrm{w}} + \rho \, w \qquad \text{at } z = \eta. \qquad (32)$$

This is an Eulerian version of the material kinematic boundary condition of equation (28).

3. TRACER BUDGET

The tracer concentration C is defined to be the mass of tracer per mass of seawater for material tracers such as salt or biogeochemical tracers. Hence, the total tracer mass within a finite region of seawater is given by the integral $\int C \rho \, \mathrm{d}V$. The

Figure 2. Schematic of the ocean's upper surface with a smoothed undulating surface at $z = \eta(x, y, t)$ and outward normal direction $\hat{\mathbf{n}}_\eta$. Undulations of the surface height are on the order of a few meters due to tidal fluctuations in the open ocean and order 10–20m in certain embayments (e.g., Bay of Fundy in Nova Scotia). When imposing the weight of sea ice onto the ocean surface, the surface height can be depressed even further, on the order of 5–10m, with larger values possible in some cases. It is important for simulations to employ numerical schemes facilitating such wide surface height undulations.

which is equivalent to the no-normal-flow boundary condition $\mathbf{v} \cdot \hat{\mathbf{n}} = 0$.

At the ocean surface, mass transport arises from the passage of water across the penetrable free surface. We define this transport as

$$(\text{mass/time}) \text{ through surface} = Q_w^\eta \, \mathrm{d}A_\eta, \qquad (25)$$

with Q_{w}^η the mass flux through the ocean surface, normalized by the area element $\mathrm{d}A_\eta$ on the surface. We next exploit the assumption that the surface interface of ocean models has no overturns, in which case we can introduce the horizontal area $\mathrm{d}A$ to rewrite the mass flux as

$$(\text{mass/time}) \text{ through surface} \equiv Q_w \, \mathrm{d}A. \qquad (26)$$

Q_{w} is the mass flux used in ocean models, with some models defining

$$Q_{\mathrm{w}} = \rho_{\mathrm{w}} q_{\mathrm{w}} \qquad (27)$$

where ρ_{w} is the density of the water crossing the ocean surface, and q_{w} is the fresh water flux (with units of velocity).[3]

To develop the surface kinematic boundary condition (Figure 2), we note that the free surface, defined at $z - \eta(x, y, t) = 0$, materially evolves according to the flux of mass crossing it so that

material evolution of tracer mass within a Lagrangian parcel of mass conserving fluid is given by

$$\rho \frac{dC}{dt} = -\nabla \cdot \mathbf{J} + \rho \mathcal{S}, \qquad (33)$$

where S is a tracer source that cannot be written as the convergence of a flux. There are many biogeochemical tracers that have a non-trivial S. The tracer flux $\mathbf{J}$ arises from subgrid-scale (SGS) transport of tracer occurring in the absence of mass transport. Such transport consists of SGS diffusion and advection. Use of the identity (7) allows us to bring the Lagrangian parcel tracer budget (33) into the following Eulerian flux form

$$(\rho C)_{,t} + \nabla \cdot (\rho \mathbf{v} C + \rho \mathbf{F}) = \rho S, \qquad (34)$$

where $\mathbf{J} = \rho \mathbf{F}$ introduces the tracer concentration flux $\mathbf{F}$, with dimensions velocity $\times$ tracer concentration.

As the tracer flux $\mathbf{J}$ and tracer source S are not associated with mass transport or mass sources, they both vanish when the tracer concentration is uniform, in which case the tracer budget of equation (34) reduces to the mass budget of equation (5). This compatibility relation between mass and tracer budgets follows trivially from the definition of tracer concentration. It forms an important guiding principle that a numerical algorithm must maintain in order for the simulation to conserve tracer. Not all ocean models satisfy this constraint, in which case they suffer from local or global tracer non-conservation [*Griffies et al.*, 2001; *Campin et al.*, 2004; *White et al.*, 2007].

In a manner analogous to the definition of a dia-surface velocity component in Section 2.2, it is useful to identify the amount of tracer transported through a surface from the effects of SGS processes as follows:

$$\frac{\text{(SGS tracer mass through surface)}}{\text{time}} = dA_{(\hat{\mathbf{n}})} \, \hat{\mathbf{n}} \cdot \mathbf{J}. \quad (35)$$

For this purpose, we are led to introduce the dia-surface SGS tracer flux

$$J^{(s)} \quad \equiv \quad \frac{dA_{(\hat{\mathbf{n}})} \, \hat{\mathbf{n}} \cdot \mathbf{J}}{dA} \qquad (36)$$

$$= \quad z_{,s} \nabla s \cdot \mathbf{J} \qquad (37)$$

$$= (\hat{\mathbf{z}} - \nabla_s z) \cdot \mathbf{J}, \qquad (38)$$

where $\nabla_s \, z$ is the slope vector for the generalized surface introduced following equation (20). In words, $J^{(s)}$ is the tracer mass per time per horizontal area penetrating surfaces of constant generalized vertical coordinate by processes that

are unresolved by the dia-surface velocity component $w^{(s)}$. At the ocean boundaries, $J^{(s)}$ embodies the transport of tracer into the ocean from other components of the climate system.

4. LINEAR MOMENTUM BUDGET

The linear momentum of a fluid parcel is given by $\mathbf{v}\rho dV$. Through Newton's Second Law of Motion, momentum changes in time due to the influence of forces acting on the parcel. There are two external (or body) forces and two internal (or contact) forces acting on a fluid parcel that concern ocean modelers. Body forces act throughout the fluid media, with gravitational and Coriolis forces of concern.[5] Contact forces act on the volume of a continuous media by acting on the boundaries of the media. Pressure and friction are the two contact forces of concern here. Through the Green–Gauss theorem of vector calculus, the contact forces are transformed into body forces, which provides a means to formulate the equations of motion for an infinitesimal fluid parcel.

4.1. Gravitational Force and Spherical Geometry

The effective gravitational force is noncentral due to the Earth's rotation and due to inhomogeneities in the Earth's mass distribution. Hence, if the Earth were an ideal fluid, matter would flow from the poles toward the equator, thus ensuring that the Earth's surface would everywhere be perpendicular to the effective gravitational acceleration, $\mathbf{g}$. Indeed, the Earth does exhibit a slight equatorial bulge. However, inhomogeneities in the Earth's composition and surface loading by continents, glaciers, and seawater make its shape differ from the ideal case. For purposes of global ocean modeling, we ignore the inhomogeneities, but we do not ignore the equatorial bulge.

Veronis [1973], *Phillips* [1973], and *Gill* [1982] discuss how the Earth's geometry can be well approximated by an oblate spheroid, with the equatorial radius larger than the polar due to centrifugal effects. With this geometry, surfaces of constant geopotential are represented by surfaces with a constant oblate spheroid radial coordinate [page 662 of *Morse and Feshbach*, 1953]. However, the oblate spheroidal metric functions, which determine how to measure distances between points on the spheroid, are less convenient to use than the more familiar spherical metric functions. To provide a simpler form of the equations of motion on the Earth, *Veronis* [1973] and *Gill* [1982] (see in particular page 91 of Gill) indicate that it is possible, within a high level of accuracy, to maintain the best of both situations. That is, surfaces of constant r are interpreted as best fit oblate spheroidal geopotentials, yet the metric functions used to measure distance between points in the surface are approximated as spheri-

cal. As the metric functions determine the geometry of the surface, and hence the form of the equations of motion, the equations are exactly those which result when using spherical coordinates on a sphere. Hence, throughout this chapter, the geometry of the Earth is spherical, yet the radial position r represents a surface of constant geopotential, which is approximated by an oblate spheroid.

In summary, the gravitational field most convenient for ocean modeling is an effective gravitational field, which incorporates the effects from the centrifugal force. The effective gravitational field is conservative so that the gravitational acceleration of a fluid parcel can be represented as the gradient of a scalar,

$$g = -\nabla \Phi, \tag{39}$$

with Φ the geopotential. As $(\rho dV)\Phi$ is the gravitational potential energy of a parcel, Φ is also the gravitational potential energy per mass. In most ocean modeling applications, the local vertical direction is denoted by z, with $z = 0$ the surface of a resting ocean, in which case

$$\Phi \approx g z, \tag{40}$$

with $g \approx 9.8 \text{m s}^{-2}$ the acceleration due to gravity, which is generally assumed constant for ocean climate modeling. This assumption is not fundamental and can be readily jettisoned, as indeed is important for accurate ocean tide calculations.

4.2. Coriolis Force

Ocean models generally are written in the reference frame of an observer at a fixed lateral position on the rotating Earth. This moving reference frame then leads to a Coriolis force per mass, which is written [*Marion and Thornton*, 1988; *Gill*, 1982]

$$\mathbf{F}_c = -2\mathbf{\Omega} \wedge \mathbf{v}. \tag{41}$$

The Earth's rotational vector $\mathbf{\Omega}$ points outward through the north pole, with the Earth's rotation counterclockwise if looking down onto the north pole.

The Earth's angular velocity is comprised of two main contributions: the spin of the Earth about its axis and the orbit of the Earth about the Sun. Other astronomical motions can be neglected for ocean modeling. Therefore, in the course of a single period of 24 h, or $24 \times 3600 = 86400$ s, the Earth experiences an angular rotation of $(2\pi + 2\pi/365.24)$ radians, in which case the angular velocity of the Earth is approximated by

$$\Omega = \left(\frac{2\pi + 2\pi/365.24}{86400 \text{s}} \right)$$

$$= \left(\frac{\pi}{43082} \right) \text{s}^{-1}$$

$$= 7.2921 \times 10^{-5} \text{s}^{-1}. \tag{42}$$

For the purposes of ocean modeling, this angular velocity can be assumed constant in time.

4.3. Stresses From Pressure and Friction

When parcels exchange momentum with other parcels and/or boundaries, this exchange can be represented by the components of a symmetric stress tensor whose elements have units of a force per area. There are two types of stress of concern for ocean fluid dynamics: diagonal stresses associated with pressure p and stresses associated with friction organized into the components of a symmetric and trace-free frictional stress tensor τ. The frictional stress tensor is also known as the deviatoric stress tensor [e.g., *Aris*, 1962; *Batchelor*, 1967] because it represents deviations from the static case when stress is due solely to pressure.

The contact force from friction and pressure acting on the boundaries of a fluid region can generally be written

$$\mathbf{F}_{\text{stress}} = \int (\tau \cdot \hat{\mathbf{n}} - p\hat{\mathbf{n}}) \, dA_{(\hat{\mathbf{n}})}. \tag{43}$$

The surface integral is taken over the bounding surface of the domain whose outward normal is $\hat{\mathbf{n}}$. Pressure acts on a surface in the direction opposite to the outward normal, and so always acts in a compressive manner (Figure 3). Deviatoric stresses create more general forces on the surface, which can have compressive, expansive, and/or shearing characteristics. It is notable that the mechanical pressure considered here is the same as the pressure used for equilibrium and non-equilibrium thermodynamical considerations (Section 7).

The Green–Gauss theorem of vector calculus can be used to convert the area integral in equation (43) to a volume integral so that

$$\mathbf{F}_{\text{stress}} = \int \nabla \cdot (\tau - \mathbf{I}p) \, dV, \tag{44}$$

where $\mathbf{I}$ is the identity tensor. This is a fundamental result of practical relevance in the formulation of pressure forces in ocean models. That is, one may choose to formulate the
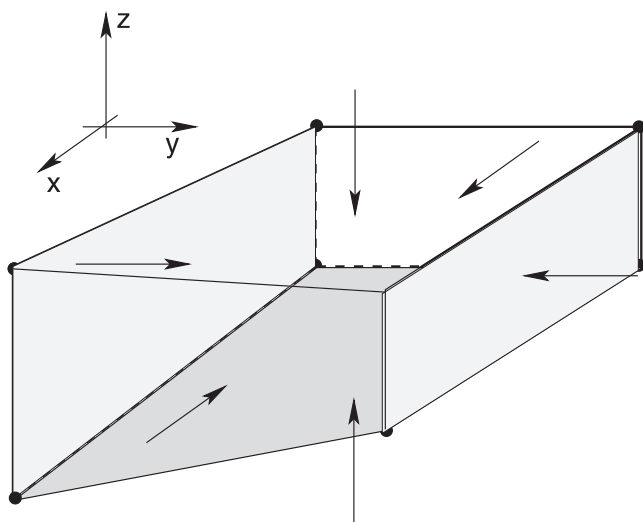
Figure 3. Schematic of a grid cell bounded at its top and bottom in general by sloped surfaces and vertical side walls. The top and bottom surfaces can represent linear piecewise approximations to surfaces of constant generalized vertical coordinates, with $s = s_1$ at the top surface and $s = s_2$ at the bottom surface. They could also represent the ocean surface (for the top face) or the ocean bottom (for the bottom face). The *arrows* represent the pressure contact forces which act in a compressive manner along the boundaries of the grid cell and in a direction normal to the boundaries. These forces arise from contact between the shown fluid volume and adjacent regions. Due to Newton's Third Law, the pressure acting on an arbitrary fluid parcel **A** due to contact with a parcel **B** is equal and opposite to the pressure acting on parcel **B** due to contact with parcel **A**. If coded according to finite volume budgets, as in *Lin* [1997], this law extends to the pressure forces acting between grid cells in an ocean model.

pressure force as the gradient of pressure integrated over the volume of the cell, as in equation (44), or as the accumulation of pressure forces acting on the boundary of the cell, as in equation (43). Both formulations are equivalent in the continuum. However, certain discrete formulations break the symmetry. For example, the finite difference approach of *Bryan* [1969a] uses an energetically consistent formulation of the pressure gradient, yet the energy-consistent method is not equivalent to a contact force formulation. In contrast, *Lin* [1997] proposes to use a finite volume formulation [e.g., chapter 6 of *Hirsch*, 1988] in which the contact force formulation (written as a closed contour integral) is constructed to be equivalent to a finite volume formulation of the pressure gradient.

The frictional stresses in a fluid arise from strains acting in the horizontal and vertical directions which, through the assumptions of a Newtonian fluid, are directly proportional to stress. The proportionality is in the form of a viscous tensor.

The stress tensor is symmetric, reflecting the inability of internal stresses to impart a net angular momentum on a fluid.

Anticipating the kinetic energy discussion in Section 6.1, we note that stresses arising from molecular viscosity dissipate kinetic energy. This result places a constraint on the form of the viscous tensor, and it motivates the name frictional stress tensor, as friction generally dissipates mechanical energy. To illustrate this property mathematically, consider friction arising from molecular viscosity to be represented in a Laplacian form and assume a planar geometry to simplify the tensor analysis. In this case, the inner product of velocity and the friction vector, which appears in the kinetic energy budget [equation (67)], can be written

$$
\begin{aligned}
\mathbf{v} \cdot \nabla \cdot \boldsymbol{\tau} &= v_m \left(\gamma v_{m,n} \right)_{,n} \\
&= \nabla \cdot \left(\gamma \nabla K \right) - \gamma \mathbf{v}_{,m} \cdot \mathbf{v}_{,m}.
\end{aligned} \tag{45}
$$

In this equation, a comma represents a partial derivative, and repeated indices are summed over their range from 1,2,3. The strength of the Laplacian friction operator is scaled by the non-negative number γ, which is the molecular dynamic viscosity for water. Typical values are around $\gamma \approx 10^{-3}$ kg m^{-1} s^{-1} [*Gill*, 1982]. More commonly considered in applications is the kinematic viscosity

$$
v = \gamma / \rho, \tag{46}
$$

whose values for water are around $v \approx 10^{-6}$ m^2 s^{-1}. The negative semi-definite term in equation (45) thus represents a kinetic energy sink associated with local viscous dissipation. It is termed Joule heating, as it represents a conversion of mechanical energy to heat (Sections 6.3 and 7.1). It is commonly written as

$$
\epsilon = v \, \mathbf{v}_{,m} \cdot \mathbf{v}_{,m} \geq 0. \tag{47}
$$

As noted by *McDougall* [2003], frictional dissipation in the ocean interior associated with molecular viscosity is on the order[6]

$$
\epsilon \approx 10^{-9} \, \mathrm{W \ kg^{-1}}. \tag{48}
$$

The number 10^{-9} W kg^{-1} sounds small, as indeed it is. To put it into perspective, using the heat capacity of seawater $C_p \approx 3989$ Joules kg^{-1} K^{-1}, frictional dissipation through molecular viscosity warms seawater at a rate of less than 10^{-3} °K per hundred years. This is a negligible amount of heating from a large-scale ocean circulation perspective, and so it is commonly neglected in large-scale models.

4.4. Momentum Budget for a Parcel

With the above considerations, the equation for linear momentum of a fluid parcel takes the form

$$\rho \frac{d\mathbf{v}}{dt} + 2\Omega \wedge \rho \mathbf{v} = -\rho \nabla \Phi + \nabla \cdot (\tau - \mathbf{I}p). \qquad (49)$$

The left-hand side of this equation is the time tendency for the linear momentum per volume of a parcel, along with the Coriolis force, and the right-hand side is the sum of the gravitational, pressure, and frictional forces. The momentum equation (49) is a form of Cauchy's equation with the diagonal pressure force split from the stress tensor. Cauchy's equation becomes the Navier–Stokes equation when assuming the frictional stress is linearly proportional to the fluid strain according to a Newtonian fluid [*Aris*, 1962; *Batchelor*, 1967].

There are two general forms that the linear momentum equation (49) appears in ocean models: the advective form and the vector invariant form. The two differ by how the material time derivative is translated into an Eulerian form. The advective form exploits the identity

$$\rho \frac{d\mathbf{v}}{dt} = (\rho \mathbf{v})_{,t} + \nabla \cdot (\rho \mathbf{v}\mathbf{v}) + M(\hat{\mathbf{z}} \wedge \rho \mathbf{v}), \qquad (50)$$

where $M = v\partial_x(\ln dy) - u\partial_y(\ln dx)$ defines an advective metric frequency. Its form given here assumes that the lateral directions are described by locally orthogonal coordinates, which is the typical case for ocean fluid mechanics. For example, in spherical coordinates[7] (r, λ, ϕ), the grid cell increments are given by $dx = (r \cos \phi) d\lambda$, $dy = r d\phi$, in which case the advective metric frequency is given by $M = (u/r) \tan \phi$. Use of equation (50) in the linear momentum balance of equation (49) leads to the Eulerian budget

$$(\rho \mathbf{v})_{,t} + \nabla \cdot (\rho \mathbf{v}\mathbf{v}) + (2\Omega + \hat{\mathbf{z}}M) \wedge \rho \mathbf{v}$$
$$= -\rho \nabla \Phi + \nabla \cdot (\tau - \mathbf{I}p). \qquad (51)$$

The vector invariant form exploits the identity

$$\rho \frac{d\mathbf{v}}{dt} = \rho (\partial_t + \omega \wedge)\mathbf{v} + \rho \nabla \mathcal{K}, \qquad (52)$$

where

$$\omega = \nabla \wedge \mathbf{v} \qquad (53)$$

is the three-dimensional vorticity, and

$$\mathcal{K} = \mathbf{v} \cdot \mathbf{v}/2 \qquad (54)$$

is the kinetic energy per mass of a fluid parcel. Use of equation (52) in the linear momentum balance of equation (49) leads to the prognostic equation for the linear momentum per mass; i.e., the velocity $\mathbf{v}$

$$[\partial_t + (2\Omega + \omega) \wedge]\mathbf{v} = -\nabla \varepsilon + \rho^{-1} \nabla \cdot (\tau - \mathbf{I}p), \qquad (55)$$

where

$$\mathcal{E} = \Phi + \mathcal{K} \qquad (56)$$

is the total mechanical energy per mass of a fluid parcel. The vector invariant velocity equation (55) exposes vorticity and mechanical energy per unit mass, whereas the linear momentum equation (51) focuses on nonlinear self-advection along with the coordinate-dependent advection metric frequency.

4.5. Vorticity and Potential Vorticity

Vorticity is one of the most important dynamical variables in fluid mechanics. Furthermore, the associated potential vorticity scalar is key to understanding and predicting aspects of geophysical fluid flows. This section introduces these vorticities, with more complete discussions available in such places as *Gill* [1982], *Pedlosky* [1987], *Müller* [1995], *Salmon* [1998], and *Vallis* [2006].

To derive the vorticity equation, take the curl of the vector-invariant form of the velocity equation (55) to lead to the material evolution of absolute vorticity $\omega_a = \omega + 2\Omega$

$$\frac{d\omega_a}{dt} = \underbrace{-\omega_a (\nabla \cdot \mathbf{v})}_{\text{vortex stretching}} + \underbrace{(\omega_a \cdot \nabla) \mathbf{v}}_{\text{vortex tilting}}$$
$$+ \underbrace{\rho^{-2} (\nabla \rho \wedge \nabla p)}_{\text{baroclinicity}} + \underbrace{\nabla \wedge \mathbf{F}^{(v)}}_{\text{friction}}, \qquad (57)$$

where we wrote the friction vector in the form $\nabla \cdot \tau = \rho \mathbf{F}^{(v)}$. The four terms on the right-hand side represent various manners whereby the absolute vorticity of a parcel is modified. The names associated with these terms represent the mechanisms under which vorticity is affected. A discussion of the physics of these mechanisms is outside the scope of the present considerations. Instead, Chapter 2 of *Pedlosky* [1987] is highly recommended for garnering a physical understanding.

Ertel [1942] determined that the potential vorticity

$$\Pi = \rho^{-1} \omega_a \cdot \nabla \chi \qquad (58)$$

is materially conserved so long as the scalar χ is materially conserved and representable as just a function of density and pressure. *Müller* [1995] and *Vallis* [2006] discuss oceanographically relevant examples of χ. Ertel's potential vorticity theorem generalizes all vorticity theorems of fluid mechanics. Furthermore, the theorem provides a practical means for determining constraints on the fluid motion. In particular, potential vorticity plays a fundamental role in hydrostatic isopycnal models. *Salmon* [1998] discusses the connection of Ertel's potential vorticity conservation to the relabelling symmetry possessed by fluid parcels. In the presence of a two-component equation of state, as in the ocean, there is no materially conserved potential vorticity [*Müller*, 1995]. Nonetheless, oceanographers have made great use of approximate forms of potential vorticity, and it therefore remains of fundamental importance in modeling.

5. DENSITY

The density of seawater is an important variable to measure in the ocean and to accurately compute in an ocean model. In particular, density variations, by means of their effects on the pressure field, provide one of the most important driving forces for large-scale circulation.

Density at a point in the ocean (the in situ density) is generally a function of temperature, salinity, and pressure,

$$\rho = \rho(\theta, S, p), \qquad (59)$$

where we choose to use either potential or conservative temperature (Section 7.2) in the functional relation. This choice is more convenient than the alternative in situ temperature, as ocean models generally carry the more conservative θ as a prognostic variable rather than in situ temperature (see Section 7 for a discussion).

Equation (59) is known as the equation of state. Its precise form is determined empirically. The most accurate equation of state appropriate for ocean models has been given by *Jackett et al.* [2006]. This work is based on that of *Feistel* [1993], *Feistel and Hagen* [1995], and *Feistel* [2003]. Most ocean models are now switching to such accurate equations of state, as the earlier approximate forms, such as *Bryan and Cox* [1972], maintain a relatively narrow range of salinity variations over which the equation is valid. With ocean mod-

els of refined grid resolution and realistic fresh water forcing, it is desirable to remove such limitations, as model salinity can vary quite widely, especially near river mouths and sea ice.

The equation of state (59) is often approximated by replacing the pressure dependence with a depth dependence

$$\rho(\theta, S, p) \rightarrow \rho(\theta, S, p_o(z)), \qquad (60)$$

where $p_o(z)$ is a predefined reference pressure profile generally set as the hydrostatic pressure arising from the initial density profile (Section 9.2). Converting pressure dependence to depth dependence produces an infinite acoustic speed, which removes acoustic modes from the system (Section 8.1). A time-dependent mass conservation is retained with the approximate density of equation (60), and this density is used to define the seawater parcel mass, the tracer mass, and the linear momentum. We may choose, however, to employ a more accurate expression for density in computing pressure if the hydrostatic approximation is used (Section 9.2). The resulting fluid is termed pseudo-incompressible [*Durran*, 1999] or quasi-non-Boussinesq [*Greatbatch et al.*, 2001].

The functional relation $\rho = \rho(\theta, S, p)$ allows us to develop the material time derivative of in situ density

$$\frac{d\ln\rho}{dt} = \frac{1}{\rho c_s^2}\frac{dp}{dt} + \beta_S\frac{ds}{dt} - \alpha_\theta\frac{d\theta}{dt}. \qquad (61)$$

In this equation, we introduced the thermal expansion and saline contraction coefficients

$$\alpha_\theta = -\left(\frac{\partial\ln\rho}{\partial\theta}\right)_{p,S} \qquad (62)$$

$$\beta_S = \left(\frac{\partial\ln\rho}{\partial S}\right)_{p,\theta} \qquad (63)$$

as well as the squared sound speed

$$c_s^2 = \left(\frac{\partial p}{\partial\rho}\right)_{S,\theta}. \qquad (64)$$

It is interesting to note that when parcels mix as they are materially transported, e.g., from molecular diffusion with diffusivities κ_θ and κ_S, the potential temperature and salinity terms in equation (61) become

$$\frac{1}{\rho \, c_s^2} \frac{\mathrm{d}p}{\mathrm{d}t} + \beta_S \nabla \cdot (\kappa_S \nabla S) - \alpha_\theta \nabla \cdot (\kappa_\theta \nabla \theta) = -\nabla \cdot \mathbf{v},$$

(65)

where mass conservation in the form of equation (3) was used to replace the density derivative with velocity convergence. This equation indicates that in addition to material changes in pressure, the mixing of salinity and potential temperature act, by means of mass continuity, to balance changes in the volume of a fluid parcel. For example, absent salinity and pressure effects, raising the potential temperature of a mass conserving fluid parcel by molecular diffusion ($\nabla \cdot (\kappa_\theta \nabla \theta) >$ 0) causes an increase in the volume of a parcel (d ln(dV)/dt = $\nabla \cdot \mathbf{v} > 0$) when the thermal expansion coefficient α_θ is positive. We caution that this is a deceptively simple thought experiment, as expansion of a region of fluid by heating is actually mediated by pressure fluctuations occuring as acoustic modes, a subject we consider in Section 8.1.

6. ENERGETIC BUDGETS

There are fundamental symmetries that the momentum equation (49) respects, and these symmetries lead to conservation laws for certain combinations of dynamical variables, such as kinetic energy and total energy. In the construction of numerical models, it is often beneficial to build analogous symmetries and conservation laws into the discrete equations. Such practices have been demonstrated to yield robust algorithms and physically realizable solutions. In general, it is desirable to be able to manipulate the discretized model equations in an analogous fashion to the manipulations used in obtaining the conservation laws in the continuum. Unfortunately, it is not always possible to maintain the exact conservation laws and symmetries in the discrete equations.

6.1. Kinetic Energy Budget

Energy is a useful scalar currency in physics because the total energy of a closed system is conserved. The ocean is not closed, but instead is a forced dissipative system. Nonetheless, the governing equations are energetically self-consistent, and so it is useful to consider the energetic budgets in numerical models. We start by considering the kinetic energy of a fluid parcel, which is given by $(\rho \mathrm{d}V)\mathbf{v} \cdot \mathbf{v}/2 = (\rho \mathrm{d}V)\mathcal{K}$. Bounds on this quadratic quantity can provide indirect constraints with which to develop numerical algorithms for the momentum equation. These constraints are useful, as linear momentum is not conserved on a sphere [see Section 4.11 of *Griffies*, 2004].

The kinetic energy budget is obtained by taking the inner product of $\mathbf{v}$ with the linear momentum equation (49) to find

$$\rho \, \frac{\mathrm{d}\mathcal{K}}{\mathrm{d}t} = -\rho \, \mathbf{v} \cdot \nabla \Phi - \mathbf{v} \cdot \nabla p + \mathbf{v} \cdot \nabla \cdot \tau.$$

(66)

Use of the identity (7) renders the Eulerian budget

$$(\rho \mathcal{K})_{,t} + \nabla \cdot (\rho \mathbf{v} \mathcal{K} + \mathbf{v} p) = p \nabla \cdot \mathbf{v} - \rho \mathbf{v} \cdot \nabla \Phi + \mathbf{v} \cdot \nabla \cdot \tau.$$

(67)

Note that we could have obtained this budget by working with either of the Eulerian forms: the advective form of the momentum budget (51) or the vector invariant velocity equation (55). On the discrete lattice, it is often more convenient to work with the vector invariant form, such as commonly used with the Arakawa C-grid models [*Mesinger and Arakawa*, 1976].

Terms on the right-hand side of the kinetic energy budget (67) represent energy conversion processes, whereby kinetic energy is exchanged for other forms of energy. Recall from the discussion of mass conservation in Section 2.1, the volume of a fluid parcel expands in a diverging velocity field according to equation (2). We thus identify $p \nabla \cdot \mathbf{v}$ as a pressure work term: as pressure works to compress a fluid parcel ($p \nabla \cdot \mathbf{v} < 0$), the internal energy of the parcel increases at the cost of decreasing its kinetic energy. The term $-\rho \mathbf{v} \cdot \nabla \Phi$ represents an exchange of kinetic energy for gravitational potential energy arising from vertical motions. That is, as parcels move up the gravitational field gradient ($\rho \mathbf{v} \cdot \nabla \Phi > 0$), kinetic energy decreases as potential energy increases (see Section 6.2 for more on gravitational potential energy). Note that in the special case, common in ocean models, where the geopotential is aligned according to the local vertical, then $\nabla \Phi = g\hat{\mathbf{z}}$, and so $\rho \mathbf{v} \cdot \nabla \Phi = \rho w g$. Finally, the frictional stress term $\mathbf{v} \cdot \nabla \cdot \tau$ was discussed in Section 4.3 where we noted that equation (45) provides the form for this term due to molecular viscous effects.

Bringing these results together leads to the Eulerian budget for kinetic energy per volume of a fluid parcel

$$(\rho \mathcal{K})_{,t} + \nabla \cdot (\rho \mathbf{v} \mathcal{K} + \mathbf{v} p - \mathbf{v} \cdot \tau)$$
$$= p \nabla \cdot \mathbf{v} - \rho \mathbf{v} \cdot \nabla \Phi - \rho \epsilon.$$

(68)

In this relation, we reintroduced the more general form of the viscous transport $\mathbf{v} \cdot \tau$, which allows us to identify a kinetic energy flux

$$\mathbf{J}_{\mathcal{K}} = \rho \, \mathbf{v} \mathcal{K} + \mathbf{v} p - \mathbf{v} \cdot \tau. \qquad (69)$$

The terms in this flux alter kinetic energy locally but integrate to boundary terms when considering a global budget.

In the derivation of the local kinetic energy budget (68), the Coriolis term has exactly zero contribution to the energetics. This result follows, as the Coriolis force arises from our choice to describe motion in a moving reference frame at a point on the rotating Earth. Such an arbitrary choice of reference frame can have no impact on the energy of a parcel. This result suggests a desirable property for the discretized form of the momentum equation: that there be no local kinetic energy source due to the Coriolis force. Unfortunately, this property is difficult to achieve on the discrete lattice if components of discrete velocity reside on a staggered grid and are not co-located. The Arakawa B-grid has both horizontal velocity components co-located, whereas the Arakawa C-grid places them on adjacent cell faces [*Arakawa*, 1966]. When local conservation is unobtainable, it may still be useful to satisfy the global kinetic energy budget

$$\partial_t \int \mathcal{K} \rho \, dV = \int dV \, (p \nabla \cdot \mathbf{v} - \rho \, \mathbf{v} \cdot \nabla \Phi - \rho \epsilon), \quad (70)$$

in which we dropped boundary terms for brevity. In the case of the Coriolis force on an Arakawa C-grid, there are some discretizations that ensure there is no net global spurious source or sink of kinetic energy associated with these terms [*Sadourny*, 1975; *Arakawa and Lamb*, 1981; *Arakawa and Hsu*, 1990].

6.2. Gravitational Potential Energy Budget

The evolution of gravitational potential energy $(\rho dV)\Phi$ for a parcel follows trivially by use of mass conservation

$$(\rho \, \Phi)_{,t} + \nabla \cdot (\rho \, \mathbf{v} \Phi) = \rho \, (\partial_{,t} + \mathbf{v} \cdot \nabla) \, \Phi. \qquad (71)$$

Time dependence can arise for the geopotential through tidal effects. In this case, the energetic balances for total energy of the terrestrial ocean fluid (Section 6.3) includes a source term representing input of potential energy from the astronomical bodies affecting the tidal forcing. In addition to time-dependent effects, the potential energy of a parcel is affected by motions through the gravitational field. Namely, motions up the geopotential gradient $(\rho \mathbf{v} \cdot \nabla \Phi > 0)$ increase gravitational potential energy. This mechanical energy conversion term is equal and opposite to the corresponding conversion term in the kinetic energy budget (68).

Notably, mixing processes, which affect internal energy (Section 6.3), are absent on the right-hand side of the gravitational potential energy budget (71). Therefore, the connection between potential energy and internal energy is indirect. That is, mixing leads to local density modifications, which then lead to divergent flow through mass conservation [equation (3)]. This then leads to work being done on the fluid, which converts internal energy to kinetic energy. Then, through an adiabatic adjustment process, motions through the gravitational field are realized so as to modify potential energy. This adiabatic adjustment process is carried out very rapidly by acoustic modes (Section 8.1).

The total mechanical energy, $\mathcal{E} = \mathcal{K} + \Phi$, is the sum of kinetic and gravitational potential energies, and it evolves according to

$$(\rho \, \mathcal{E})_{,t} + \nabla \cdot (\rho \, \mathbf{v} \mathcal{E} + \mathbf{v} p - \mathbf{v} \cdot \tau) = \rho \, \Phi_{,t} + p \nabla \cdot \mathbf{v} - \rho \epsilon. \qquad (72)$$

On the left side is the divergence of the mechanical energy flux, with this flux acting to transport mechanical energy throughout the fluid. On the right side are source terms that represent time-dependent gravitational effects $(\rho \Phi_{,t})$ and the conversion between kinetic energy and internal energy.

6.3. Mechanical Plus Internal Energies

In the previous discussion, we have inferred the existence of internal energy based on the conversion of mechanical energy into a non-mechanical form. This inference is founded on an assumption that total energy of a fluid parcel is conserved. Quite generally, internal energy represents the energy of the molecular degrees of freedom that are averaged out when formulating a continuum description of a fluid. That is, the internal energy per mass, I, embodies the energy of molecular thermal agitation and molecular interactions, with details of this energy unavailable with a continuum description. Another source of energy introduced in our discussion of gravitational potential energy (Section 6.2) arises from time-dependent gravitational fields $\rho \Phi_{,t}$, which represent tidal forcing. We consider time-dependent gravitational fields as a source of energy external to the terrestrial ocean fluid.

The total energy per mass, $\mathcal{T}$ (specific energy), of a fluid is therefore written as the sum of the mechanical plus internal energies

$$\mathcal{T} = \mathcal{K} + \Phi + \mathcal{I}, \qquad (73)$$

where, again, $\mathcal{K} = \mathbf{v}^2/2$ is the kinetic energy per mass of a fluid parcel, Φ is the gravitational potential energy per mass, and $\mathcal{I}$ is the internal energy per mass. Energy conservation for a fluid parcel means that total energy per mass evolves according to the conservation law

$$(\rho\, \mathcal{T})_{,t} + \nabla \cdot \mathbf{J}_{\mathcal{T}} = \rho\, \Phi_{,t} \qquad (74)$$

for some flux of energy $\mathbf{J}_{\mathcal{T}}$. Nonzero normal flux components arise for open fluid systems such as the ocean. Again, the nonzero source term $\rho\Phi_{,t}$ arises from gravitational effects external to the terrestrial ocean system.

   Based on considerations of mechanical energy flux for a parcel affected by friction, we define the flux of total energy as

$$\mathbf{J}_{\mathcal{T}} = \rho\, \mathbf{v}\mathcal{E} + \mathbf{v}p - \mathbf{v}\cdot\tau + \mathbf{J}_q. \qquad (75)$$

We introduced here the heat flux $\mathbf{J}_q$, which is generally a function of temperature as well as tracer concentration [for discussions, see *Fofonoff*, 1962; *Gregg*, 1984; *Landau and Lifshitz*, 1987; *Davis*, 1994; *McDougall*, 2003]. Subtracting the mechanical energy budget (72) from the total energy budget (74) leads to the internal energy budget for a fluid parcel

$$\rho\, \frac{\mathrm{d}\mathcal{I}}{\mathrm{d}t} = -\nabla \cdot \mathbf{J}_q - p\,\nabla\cdot\mathbf{v} + \rho\,\epsilon. \qquad (76)$$

Internal energy of a parcel is thus affected by the convergence of heat fluxes and sources due to pressure work and frictional dissipation. Notice how internal energy is increased by pressure work acting to compress the fluid. In the absence of irreversible effects due to heat transport and friction, internal energy is affected only by pressure work. Notably, equation (76) is a reflection of the First Law of Thermodynamics applied to a moving fluid parcel assumed to be locally in thermodynamic equilibrium, but non-locally to be out of equilibrium. We have more to say on such applications of linear irreversible thermodynamics to a moving fluid in Section 7.

7. BASIC NON-EQUILIBRIUM THERMODYNAMICS

   The equations of an ocean model embody Newton's Laws of motion applied to a continuum fluid. Additionally, they employ results from linear irreversible, or non-equilibrium, thermodynamics, which is the subject of this section. In particular, it is useful to work with a thermodynamic variable that is readily measured, provides information about the heat of a fluid parcel, and is conservatively transported through the fluid. However, there is no strictly conservative thermodynamic scalar that measures heat, as there are always sources, such as from frictional dissipation or heat of mixing. The purpose of this section is to introduce some

basic notions of non-equilibrium thermodynamics and, in the process, expose a few details about useful temperature variables.

7.1. Budgets for Entropy and In Situ Temperature

   We start the discussion with the fundamental thermodynamic relation [see, for example, Section 5.2.4 of *Griffies*, 2004]

$$\mathrm{d}\mathcal{I} = T\,\mathrm{d}\zeta - p\,\mathrm{d}\rho^{-1} + \mu_S\,\mathrm{d}S, \qquad (77)$$

where T is the in situ temperature, ζ is the entropy per mass, $1000\mu_S = \mu_{\mathrm{salt}} - \mu_{\mathrm{water}}$ is the relative chemical potential between salt and fresh water.[8] This relation holds between infinitesimal changes in thermodynamical state functions. Hence, although derived for quasi-static processes from the First Law of Thermodynamics using connections to work and heat, equation (77) holds for arbitrary infinitesimal changes; its connection to the First Law of Thermodynamics holds only for quasi-static processes.

   Now assume that each fluid parcel is in local thermodynamic equilibrium yet allow the full ocean system to be out of equilibrium. These assumptions yield the following internal energy time evolution

$$\rho\, \frac{\mathrm{d}\mathcal{I}}{\mathrm{d}t} = \rho\, T\, \frac{\mathrm{d}\zeta}{\mathrm{d}t} - p\,\nabla\cdot\mathbf{v} + \rho\,\mu_S\, \frac{\mathrm{d}S}{\mathrm{d}t}, \qquad (78)$$

where we used the mass balance (3) to relate material changes in density to the velocity convergence. The result (78) allows one to transfer the methods of equilibrium thermodynamics to the non-equilibrium or linear irreversible thermodynamics of moving fluid parcels. The term linear in this name refers to an assumption that the system is close to thermodynamic equilibrium. In this case, the dissipative thermodynamic fluxes are linear functions of the gradients of the thermodynamic state variables. Nonlinear effects are not absent, however, as there are nonlinear effects from advective transport, nonlinear source terms, a nonlinear equation of state, and nonlinear dependence of the transport coefficients. *DeGroot and Mazur* [1984] provide a thorough accounting of this subject, and *Gregg* [1984] and *Davis* [1994] apply these methods to small-scale mixing in the ocean. Slightly different formulations can be found in *Batchelor* [1967] and *Landau and Lifshitz* [1987], and their approaches are preferred in the following.

   Using equation (76) for the evolution of internal energy in equation (78) leads to the expression for evolution of entropy in a seawater parcel

$$T \rho \frac{\mathrm{d}\zeta}{\mathrm{d}t} = -\nabla \cdot \mathbf{J}_q + \rho \, \varepsilon - \rho \, \mu_{\mathrm{S}} \frac{\mathrm{d}S}{\mathrm{d}t}. \qquad (79)$$

This equation implies that entropy of a fluid parcel evolves by three irreversible mixing processes: (1) convergence of heat fluxes; (2) frictional dissipation sources that increase a parcel's heat content by Joule heating; and (3) salinity mixing. Correspondingly, a parcel generally maintains constant entropy if processes associated with its evolution are adiabatic, frictionless, and isohaline. As the friction source is very small in the ocean, adiabatic isohaline transport is very nearly isentropic. Indeed, when ocean modelers refer to adiabatic and isohaline processes, they typically assume this to be synonymous with isentropic.[9]

We now expose a few steps along the path toward developing a scalar field whose evolution is approximately conservative and which provides a measure of heat in the ocean. For this purpose, we develop an equation for the evolution of in situ temperature. To start, note that specific entropy ζ can be considered a function of pressure, temperature, and salinity $\zeta(p, T, S)$. Consequently, its incremental change is given by

$$\mathrm{d}\zeta = \zeta_{,p} \, \mathrm{d}p + \zeta_{,T} \, \mathrm{d}T + \zeta_{,S} \, \mathrm{d}S, \qquad (80)$$

with each of the partial derivatives taken with the other independent variables held fixed. Use of the following Maxwell thermodynamic relations

$$\rho \left(\frac{\partial \zeta}{\partial p} \right)_{T,S} = -\alpha_T \qquad (81)$$

$$\left(\frac{\partial \zeta}{\partial S} \right)_{T,p} = -\frac{\partial \mu_S}{\partial T} \qquad (82)$$

leads to

$$\rho T \, \mathrm{d}\zeta = -T \, \alpha_T \, \mathrm{d}p + \rho \, C_{\mathrm{pS}} \, \mathrm{d}T - \rho \, T \frac{\partial \mu_S}{\partial T} \, \mathrm{d}S, \qquad (83)$$

where we introduced the following thermodynamic response functions

$$C_{\mathrm{pS}} = T \left(\frac{\partial \zeta}{\partial T} \right)_{p,S} \qquad (84)$$

$$\alpha_T = -\left(\frac{\partial \ln \rho}{\partial T} \right)_{p,S}, \qquad (85)$$

with C_{pS} the specific heat with constant pressure and salinity and α_T the thermal expansion coefficient for in situ temperature [in contrast to that defined for potential temperature or

conservative temperature used in equation (62)]. As for deriving the internal energy equation (78), assume local thermodynamic equilibrium for parcels, thus allowing relation (83) to hold for material parcels moving through the fluid, in which case

$$\rho \, C_{\mathrm{pS}} \frac{\mathrm{d}T}{\mathrm{d}t} = \rho \, T \frac{\mathrm{d}\zeta}{\mathrm{d}t} + T \, \alpha_T \frac{\mathrm{d}p}{\mathrm{d}t} - \rho \, T \frac{\partial \mu_S}{\partial T} \frac{\mathrm{d}S}{\mathrm{d}t}. \qquad (86)$$

Now employ the relation (79) for entropy evolution to render

$$\rho \, C_{\mathrm{pS}} \frac{\mathrm{d}T}{\mathrm{d}t} = T \, \alpha_T \frac{\mathrm{d}p}{\mathrm{d}t} + \rho \left(\mu_S - T \frac{\partial \mu_S}{\partial T} \right) \frac{\mathrm{d}S}{\mathrm{d}t} + \rho \epsilon - \nabla \cdot \mathbf{J}_q. \qquad (87)$$

Temperature of a seawater parcel is thus affected by the following processes: (1) adiabatic pressure effects which alter the temperature by expansion or contraction of the parcel, (2) material changes in salinity, (3) Joule heating from frictional dissipation, and (4) the convergence of heat fluxes. It is possible to remove the adiabatic compression effects by introducing potential temperature (Section 7.2). However, the remaining source terms cannot in general be absorbed into another scalar function.

7.2. Potential and Conservative Temperatures

Vertical motion made without changes to entropy or salinity change the hydrostatic pressure of a fluid parcel, which causes its in situ temperature to change according to [see equation (83)]

$$\mathrm{d}T = \Gamma \, \mathrm{d}p, \qquad (88)$$

where $\Gamma = (T\alpha_T)/(\rho C_{\mathrm{pS}})$ is the adiabatic lapse rate. Consequently, in situ temperature is not a conservative thermodynamic variable to label water parcels of common origin, as it changes even in the absence of mixing or heating. This observation leads one to consider removing adiabatic pressure effects from in situ temperature.

Potential temperature is defined as the in situ temperature that a water parcel of fixed composition would have if isentropically transported from its in situ pressure to a reference pressure p_r, with the reference pressure typically taken at the ocean surface. Mathematically, the potential temperature θ is the reference temperature obtained by integration of $\mathrm{d}T = \Gamma \mathrm{d}p$ for an isentropic and isohaline in situ temperature change with respect to pressure [e.g., *Apel*, 1987]:

$$\theta(S, T, p; p_r) = T + \int_p^{pr} \Gamma(S, \theta, p') \, \mathrm{d}p'. \qquad (89)$$

By definition, the in situ temperature, T, equals the potential temperature, θ, at the reference pressure $p = p_r$. Elsewhere, these two temperature fields differ by an amount determined by the adiabatic lapse rate. The potential temperature of a parcel is constant when the entropy and material composition of the parcel are constant. Mathematically, this result follows by noting that when entropy changes at a fixed pressure and composition, $p = p_r$, then in situ temperature equals potential temperature. Equation (83) then leads to

$$\mathrm{d}\zeta = C_{\mathrm{pS}} \, \mathrm{d}\ln\theta, \qquad (90)$$

implying $\mathrm{d}\zeta = 0$ if and only if $\mathrm{d}\theta = 0$.

Potential temperature has proven useful for many oceanographic purposes. However, we have yet to ask whether it is a convenient variable to mark the heat content in a parcel of seawater. Traditionally, the potential temperature multiplied by the heat capacity is used for this purpose. *Bacon and Fofonoff* [1996] provide a review with suggestions for this approach. In contrast, *McDougall* [2003] argues that potential temperature multiplied by heat capacity is less precise, by some two orders of magnitude, than an alternative thermodynamic tracer called potential enthalpy. Indeed, enthalpy is what is more commonly associated with heat in thermodynamics [*Fofonoff*, 1962], so it is sensible that ocean models should be carrying an enthalpy variable to represent heat content.

At present, most ocean models consider their heat variable to be potential temperature, and this variable is assumed to be conservative. This assumption has implications for the equation of state (59) and the calculation of heat fluxes at the ocean boundaries. *McDougall* [2003] notes that if we reinterpret the conservative heat variable in a model to be proportional to potential enthalpy, then the conservation equation

$$\rho\, C_p^o\, \frac{\mathrm{d}\Theta}{\mathrm{d}t} = -\nabla \cdot \mathbf{J}_q \qquad (91)$$

is an approximate statement of the first law of thermodynamics for the ocean. In this equation, Θ is the conservative temperature variable, and C_p^o is an appropriately chosen constant heat capacity. The alternative to equation (91), whereby Θ is replaced by potential temperature θ, is commonly used by ocean modelers. It is roughly 100 times less accurate and can lead to sea surface temperature differences upwards of 1°C in regions of large salinity deviation, such as river mouths. The National Aeronautics and Space Administration Goddard Institute for Space Studies ocean model [*Russell et al.*,

1995] uses potential enthalpy for its heat variable, and the new version of the Modular Ocean Model [*Griffies*, 2007] provides an option for using conservative temperature. For the remainder of this document, we use potential temperature θ as the heat scalar, noting that the equations remain the same if using the more accurate Θ.

8. LINEAR MODES OF MOTION

Having now developed the fundamental equations of the ocean, we move on to the task of introducing the linear dynamical modes admitted by these equations. This analysis initiates an exploration of the multitude of dynamical processes active in the ocean. More central to our purposes, the analysis provides us with guidance toward which numerical methods are needed to integrate the equations. The results are generally used to motivate certain approximations, so some material here anticipates approximation methods discussed in Section 9.

We are particularly interested here in the speed of various linear dynamical modes. This then allows us to determine a guide for the time step required to explicitly represent a particular mode by making use of the Courant–Friedrichs–Lewy (CFL) constraint [e.g., *Haltiner and Williams*, 1980; *Durran*, 1999]. Depending on details of space and time discretization, this constraint says that when simulating a propagating signal on a discrete lattice, $U\Delta t/\Delta$ must remain less than a number on the order of unity. Here, U is the speed of the mode, Δ is the discrete grid spacing, and Δt is the discrete time step. The CFL constraint says that as motions increase in speed, the numerical model must reduce its time step to represent these motions. Finer grid spacings also require smaller time steps. If the model fails to satisfy the CFL constraint for a particular mode, the model will likely go unstable, and it generally will do so quite rapidly.

8.1. Acoustic Waves

Linear acoustic fluctuations arise from small amplitude adiabatic, frictionless, and isohaline motion [e.g., *Apel*, 1987]. Such motions lead, through the equation of state (59), to the equation for pressure fluctuations in terms of density fluctuations [see equation (61)]

$$\frac{\mathrm{d}p}{\mathrm{d}t} = \rho\, c_s^2\, \frac{\mathrm{d}\ln\rho}{\mathrm{d}t}. \qquad (92)$$

Noting the approximate form of mass conservation in Section 9, we write mass conservation in the form

$$\epsilon_{nb} \frac{d \ln \rho}{dt} = -\nabla \cdot \mathbf{v}, \tag{93}$$

where we introduced the non-dimensional parameter ϵ_{nb}, with $\epsilon_{nb} = 1$ with mass conserving non-Boussinesq kinematics and $\epsilon_{nb} = 0$ for incompressible flow. Likewise, we write the linearized velocity equations, in the absence of the Coriolis force, friction, and gravity force, in the form

$$\rho \, \mathbf{u}_{,t} = -\nabla_z p \tag{94}$$

$$\epsilon_{nh} \rho \, w_{,t} = -p_{,z} \tag{95}$$

where ∇_z is the horizontal gradient operator, and we introduced the non-dimensional parameter ϵ_{nh}, which is unity for non-hydrostatic dynamics and vanishes for hydrostatic dynamics. Use of these relations in a linearized version of the pressure equation (92) leads to the wave equation for linear pressure fluctuations[10]

$$[\epsilon_{nb} \, \epsilon_{nh} \, \partial_{tt} - c_s^2 \, (\epsilon_{nh} \nabla_z^2 + \partial_{zz})] \, p = 0. \tag{96}$$

Considering a single Fourier mode with space–time dependence of the form $\exp[i(\omega t - kx - ly - mz)]$, an approximate modal analysis of the above system yields the dispersion relation involving two of the four modes to be of the form

$$\left(\frac{\epsilon_{nh} \, \epsilon_{nb}}{c_s^2} \right) \omega^2 = \epsilon_{nh} \, (k^2 + l^2) + m^2. \tag{97}$$

The unapproximated system (with $\epsilon_{nb} = \epsilon_{nh} = 1$) has non-dispersive modes that travel at speed c_s in three dimensions. The phase speed $c_s \sim 1500 \mathrm{ms}^{-1}$ in the ocean is roughly two orders of magnitude faster than motions of interest in most climate and regional applications. If these modes were explicitly represented in models, then the time step would be very small, making the model prohibitively expensive.

There are three distinct ways in which the acoustic modes can be "filtered" from the system.

1. Make the equation of state (59) independent of pressure (incompressible), in which case $1/c_s \to 0$. This approach has the advantage that only the equation of state is modified. It has the disadvantage that it is inappropriate to neglect the effect of pressure on density at global scales [e.g., *Dewar et al.*, 1998].

2. Constrain the flow to be incompressible by setting $\epsilon_{nb} = 0$. Here, sound waves are prohibited because the acoustic mode propagation requires divergent flow to drive density and pressure anomalies. This approach, used alone, renders the system elliptic in pressure. It is the approach used in the

Massachusetts Institute of Technology general circulation model (MITgcm) when integrating the Boussinesq non-hydrostatic equations [*Marshall et al.*, 1997].

3. Assume hydrostatic (or quasi-hydrostatic) balance in the vertical momentum equation (set $\epsilon_{nh} = 0$). In this case, only the $m = 0$ mode satisfies the dispersion relation (97). This is the traditional approach in meteorology, which filters vertically propagating sound waves but retains an external acoustic mode known as the Lamb wave.

In oceanography, the traditional filters used are the second and third in conjunction. This approach filters out all acoustic modes and converts the elliptic problem for pressure into the local one-dimensional hydrostatic balance. Recently, however, non-Boussinesq ocean models are becoming the norm. In these models, only hydrostatic balance is used to filter acoustic modes, thus retaining the Lamb wave. The Lamb wave has not yet presented itself as a cause for concern in the stability of non-Boussinesq hydrostatic ocean models probably because the time-implicit or split-explicit treatment of the external mode is sufficient to damp or resolve this mode [see comment at the end of *DeSzoeke and Samelson*, 2002].

A fourth approach to numerically handling acoustic modes has been used in regional models. Here, rather than filtering the modes, the models slow them down so that they can be explicitly resolved [*Browning et al.*, 1990]. As for the first method above, this approach is likely to be inappropriate for global scale modeling.

8.2. Inertia–Gravity Waves

After the acoustic modes, the next fastest linear modes are the inertia–gravity waves. These are rotationally modified gravity waves which exist as external modes as well as an infinite range of internal modes. The external mode can be analyzed in the context of the depth-integrated Boussinesq equations or equivalently by considering a homogenous layer of constant density fluid [e.g., Sections 5.6 and 8.2 of *Gill*, 1982]. These equations are often referred to as the shallow water equations, which we write in their linear form as

$$(\partial_t + f \hat{\mathbf{z}} \wedge) \mathbf{u} = -g \nabla \eta \tag{98}$$

$$\eta_{,t} = -H \nabla \cdot \mathbf{u}, \tag{99}$$

where $\mathbf{u}$ is the horizontal velocity field in the homogeneous layer, η is the surface height fluctuation with respect to a resting fluid at $z = 0$, and H is the depth of the resting fluid, which is assumed constant for present purposes. We assume the Coriolis parameter f to be constant, which defines the f-plane approximation.

Introducing a space–time dependence of the form $\exp[i(\omega t - kx - ly)]$ leads to three linear eigenmodes. The first occurs

with zero frequency $\omega = 0$, which is the geostrophic mode where the Coriolis force balances pressure $f\hat{\mathbf{z}} \wedge \mathbf{u} = -g\nabla\eta$. The geostrophic mode is a stationary mode of variability. It therefore places no time step constraint on the simulation. However, it is a critical element determining the large-scale structure of the ocean circulation. The nonzero frequency modes satisfy the dispersion relation

$$\omega^2 = f^2 + gH(k^2 + l^2). \tag{100}$$

The waves satisfying this relation are a pair of dispersive inertia–gravity or Poincaré waves. These waves provide the mechanism by which a fluid adjusts to an imbalance which then leads to geostrophic balance.

The inability of a numerical simulation to adequately adjust by inertia–gravity waves is very often the cause of grid-scale noise. For example, models built on the Arakawa B-grid can exhibit a checkerboard mode in the surface height field, and this is a direct consequence of the grid scale gravity waves exhibiting a null mode (spurious zero frequency numerical mode) [*Mesinger*, 1973, *Killworth et al.*, 1991], that is, certain of the numerical gravity waves are spuriously static, rather than propagating. Similarly, coarse-resolution models built on the Arakawa C-grid exhibit longitudinal or latitudinal coherent noise which is a direct consequence of a null-mode associated with the numerical representation of the Coriolis force [see *Adcroft et al.*, 1999, for a review of this issue].

Regardless of the spatial treatment of the inertia–gravity modes, permitting these modes in a simulation introduces a limitation on the model time step if they are to be treated explicitly. For short waves, the phase and group speed are approximately that of surface gravity waves. In the deep open ocean, this speed is of order $\sqrt{gH} \approx 200$ ms^{-1}. Satisfying the CFL condition for these waves in a model with $\Delta = 100$ km horizontal grid spacing (roughly 1° resolution) means the time step must satisfy $\Delta t = \Delta/U \approx 500$ s. Although longer than the time step required to admit acoustic waves, this time step is far smaller than practical when considering the needs of global ocean modeling, given the present power of computers. Other approaches must be used to avoid this limitation for the full model equations (see Section 11.6).

In contrast to the short waves, long inertia–gravity waves are dominated by rotation ($w^2 \sim f^2$). In this case, we are led to a time step limitation as a function of the Coriolis parameter. The most stringent limitation arising from these inertial waves occurs at the pole, where $1/(2\Omega) \sim 1.9$ h.

We now consider internal modes in which stratification is relevant. For this purpose, consider the following linear Boussinesq non-hydrostatic system

$$\rho_o(\partial_t + f\hat{\mathbf{z}} \wedge)\mathbf{u} = -\nabla_h p \tag{101}$$

$$\epsilon_{nh} w_{,t} + g + p_{,z}/\rho = 0 \tag{102}$$

$$\nabla \cdot \mathbf{u} + w_{,z} = 0 \tag{103}$$

$$\rho_{,t} - (N^2 \rho_o/g)w = 0, \tag{104}$$

where ρ_0 is the constant Boussinesq reference density, and we again introduce a non-dimensional parameter ϵ_{nh} to monitor non-hydrostatic effects. We ignore horizontal density variations because our focus is on effects of vertical stratification as represented by the squared buoyancy frequency

$$N^2 = -(g/\rho_o)\rho_{,z}, \tag{105}$$

which is assumed constant for present purposes. A linear modal analysis assuming a space–time dependence of the form $\exp[i(\omega t - kx - ly - mz)]$ leads to both the geostrophic mode ($\omega = 0$) and the internal inertia-gravity wave dispersion relation

$$\left(\epsilon_{nh}(k^2 + l^2) + m^2\right)\omega^2 = m^2 f^2 + (k^2 + l^2)N^2. \tag{106}$$

Non-hydrostatic effects are generally relevent only for regimes where the aspect ratio (ratio of vertical to horizontal scales) is order unity, meaning the horizontal wave numbers are on the order of the vertical: $k^2 + l^2 \approx m^2$. These modes are responsible for allowing the fluid to adjust toward geostrophic balance as well as to adjust to hydrostatic balance in the case of non-hydrostatic models. For hydrostatic inertia–gravity waves, the long waves are dominated by rotation, as were the external waves, while short waves have phase speed approaching the internal wave speed, N/m.

8.3. Rossby Waves

Rossby waves represent a slowly evolving, nearly geostrophic fluctuation. They arise from the gradient of the Coriolis parameter [see equation (121) for definition of Coriolis parameter] with respect to latitude

$$\beta = f_{,y}$$
$$= (2\Omega/R)\cos\phi. \tag{107}$$

To develop the dispersion relation for Rossby waves, reconsider the linear shallow water system of equations (98) and (99), only now, let the Coriolis parameter be given by a linear function of latitude $f = f_o + \beta y$, with f_o and β constant. Assuming a space–time dependence of the form

exp[$i(\omega t - kx - ly)$] leads to the dispersion relation satisfied for this beta plane shallow water system [e.g., Section 6.4 of *Cushman-Roisin*, 1994]

$$\omega = -\beta L_d^2 \left(\frac{l}{1 + L_d^2 (k^2 + l^2)} \right), \tag{108}$$

where $L_d^2 f_o^2 = gH$ defines the Rossby radius of deformation.

Spurious behavior of numerical Rossby waves can often be associated with spurious behavior of inertia–gravity waves. This arises because spurious behavior of inertia–gravity waves implies a spurious gravitational adjustment process, which in turn leads to a poor representation of the geostrophic balance for some modes. Short-scale Rossby waves are generally dissipated locally before they can propagate far. Indeed, this, and a preferred westward drift for large-scale waves, is the mechanism of western enhancement of boundary currents [*Pedlosky*, 1987]. A common numerical problem associated with Rossby waves is due to insufficient dissipation necessary to trap eastward propagating, short-scale Rossby waves. Removing this problem requires enhancing horizontal friction sufficiently to resolve the Munk boundary layer [*Munk*, 1950; *Griffies and Hallberg*, 2000; *Large et al.*, 2001]. Once inertial boundary currents are resolved, eddy–mean flow interactions and other nonlinear interactions tend to be sufficient. Further discussion of numerical representation of Rossby waves can be found in *Wajsowicz* [1986] and *Fox-Rabinovitz* [1991].

8.4. Implications for Stability of Numerical Models

The stability of numerical models depends on the choice of numerical time-integration method, the spatial discretization, and the permitted modes in the equations. Ocean models generally do not permit acoustic modes that would otherwise be prohibitive: a grid spacing of 100km would require a time step of order less than 1 min if the model admitted acoustic modes. The next fastest modes are the external gravity waves, with speeds exceeding 200m s^{-1} in the deep ocean. As discussed in Section 11.6, these modes are usually treated separately from the full three-dimensional fluctuations. We thus do not consider external modes in this section. The remaining processes may cause a numerical model to be unstable either through a direct numerical instability or through the generation or admission of excessive grid-scale noise.

A process may be directly numerically unstable in the von Neuman sense [*Durran*, 1999] if it is treated explicitly, and the shortest characteristic timescale of that process is not resolved by the model time step. Time-implicit treatment

of a process often yields unconditional numerical stability, although other considerations such as accuracy may lead to constraints on the model time step.

The simplest example of a process with an identifiable term in the equations is the inertial oscillation, for which the Coriolis term is responsible. The characteristic timescale is f^{-1}, which is shortest at the poles: $(4\pi/1\mathrm{d}ay)^{-1} \sim 1.9$ h. To resolve inertial oscillations, a time-explicit integration scheme requires that

$$f\Delta t < \gamma, \tag{109}$$

where γ is a number that depends on the details of the numerical integration scheme. We choose $\gamma = 1/2$ as a representative number. Thus, the maximum time step allowed to integrate inertial oscillations stably is $\Delta t_{max}^f = \gamma/f$. For reference, $1/(2f) \sim 57$ min is plotted in Figure 5.

Advection is characterized by a velocity scale, U. The shortest advective charactistic timescale in a numerical model is Δ/U, where Δ is the spatial grid scale and U is representative of the largest characteristic velocity. The CFL number is the ratio of this characteristic timescale to the model time step,

$$C_u = \frac{U\Delta t}{\Delta}. \tag{110}$$

This dimensionless ratio is often known as the Courant number. Most time-explicit schemes for advection require that C_u be less than a number on the order of unity, with the constraint more restrictive in higher dimensions due to the possibility of propagation diagonal to the discrete grid lines. That is, the largest time step that can support numerical stability for a given flow and grid spacing scales is

$$\Delta t_{max}^u \propto \frac{\Delta}{U}. \tag{111}$$

This result applies in all spatial directions for which advection is explicit. In practice, this constraint can be most restrictive for regions of fine vertical resolution with strong surface wind stress curls. Furthermore, the CFL criteria may be either additive or independent, again depending on the algorithm details.

The flow speed U is a result of the forcing and balances in a model simulation. It is also a function of resolution, particularly for low-resolution models. The transport of ocean boundary currents is determined by the basin-wide forcing, and numerical models respect this transport even at coarse resolution. However, if the boundary current is not resolved,

such as when there is only one cell in the current, then U becomes inversely proportional to Δ to maintain the proper transport. For the purposes of this discussion, we have chosen the profile for $U(\Delta)$ depicted in Figure 4. The corresponding limitation on time step (dashed line in Figure 5) has a Δ^1 dependence at fine resolution and a Δ^2 dependence at coarse resolution. These two resolution regimes for U and Δt^U are indicated in Table 1.

The gravest internal gravity wave (lowest vertical eigenmode) propagates with a characteristic speed $c_g \propto NH$. These waves have a grid scale characteristic time of Δ/c_g, which in turn leads to a stability constraint that Δt must be smaller than

$$\Delta t_{\max}^{c_g} \propto \frac{\Delta}{c_g}. \tag{112}$$

Unlike advection, the fastest internal wave speed is independent of resolution.

A friction operator is typically used to control noise in numerical models and to maintain a finite grid Reynolds number to keep the solution stable. Typical causes of noise include a high grid Reynolds number (i.e., velocity advection dominates accelerations) or insufficient dissipation to damp short eastward propagating Rossby waves near boundaries. As shown below, at coarse resolutions, the boundary resolution criteria dominates the need for viscosity, whereas the grid Reynolds number criteria dominates at fine resolution. Additionally, biharmonic friction operators are favored at fine resolution due to their enhanced scale selectivity, thus increasing the energetics of the flow while, ideally, maintaining a sufficient level of dissipation at the grid scale [e.g., *Semtner and Mintz*, 1977; *Griffies and Hallberg*, 2000]. Notably, a lack of sufficient friction may not immediately translate into a catastrophic model instability (i.e., model blow-up). Instead, depending on grid resolution, forcing, and numerical methods, it is possible for models to run stably, albeit with unphysically huge levels of grid noise, using very small, if not zero, interior friction.

We now consider the time step constraints introduced by the Laplacian and biharmonic friction operators. Viscous dissipation terms have a grid-scale characteristic time of Δ^2/A_2 and Δ^4/A_4, for harmonic and biharmonic viscosities, respectively. The explicit stability criteria require that the time step be smaller than
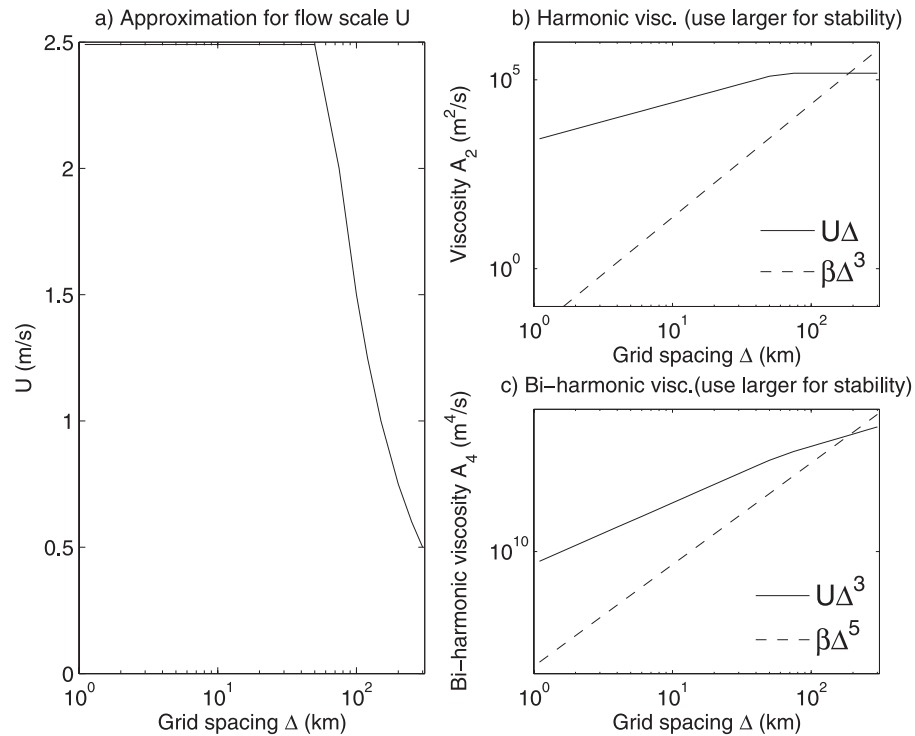

Figure 4. (**a**) Scaling for the maximum speed U seen in global numerical models as a function of spatial resolution. (**b**) The harmonic viscosity required to maintain a finite grid Reynolds number or that required to ensure the Munk boundary layer is resolved. (**c**) As for Figure 4**b**, but for a biharmonic viscosity. The spatial resolution is assumed to be isotropic and relatively uniform. This assumption is not generally the case for many global model grids.
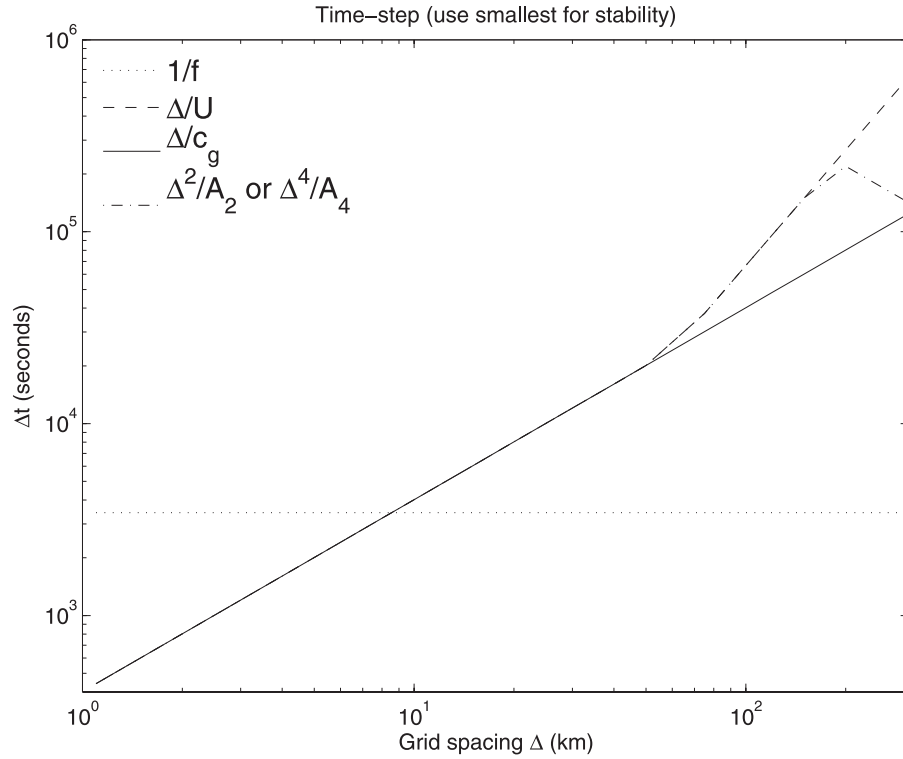
Figure 5. Using the scaling for U and viscosities shown in Figure 4, the maximum Δt allowed by each process: Coriolis term, $1/f$; advection Δ/U; internal gravity waves Δ/c_g; viscosity Δ^2/A_2 or Δ^4/A_4. Note that the timescales of processes have arbitrarily been equalized at the grid-scale, as we have neglected the details of the numerial discretizations. The curves shown can not be compared to each other, as they should each be scaled by appropriate factors to reflect the numerical details.

$$\Delta t_{\max}^{A_2} \propto \frac{\Delta^2}{A_2} \quad \text{or} \quad \Delta t_{\max}^{A_4} \propto \frac{\Delta^4}{A_4}, \tag{113}$$

respectively. These appear to have higher power dependence on Δ than the advective ($\Delta t^u_{\max}$) and gravity wave ($\Delta t^{c_g}_{\max}$) constraints. But this result is only true for given viscosity parameters (A_2 or A_4). In practice, the viscosity applied in ocean models is a strong function of resolution, and there are two distinct criteria for setting the viscosity. At very coarse resolution, a significant source of noise can occur when the viscous Munk boundary layer is not resolved [*Munk*, 1950]. The boundary layer scale, L_b, scales as

$$L_b \propto \begin{cases} \left(\dfrac{A_2}{\beta}\right)^{1/3} & \text{harmonic friction} \\[2ex] \left(\dfrac{A_4}{\beta}\right)^{1/5} & \text{biharmonic friction,} \end{cases} \tag{114}$$

where $\beta \sim 2 \times 10^{-11}$ m^{-1} s^{-1} is the planetary vorticity gradient at the equator. If we chose the viscosities to be sufficient to create a Munk boundary layer wide enough to be resolved by a grid spacing, Δ, then the viscosities will scale as

$$A_2 \propto \beta\Delta^3 \quad \text{or} \quad A_4 \propto \beta\Delta^5, \tag{115}$$

respectively.[11] This scaling determines the slope of the curves for A_2 and A_4 in the coarse grid spacing regime of Figure 4. Thus, the effective characteristic timescales [equation (113)] for viscosity becomes $(\beta\Delta)^{-1}$ for both harmonic and biharmonic forms. This scaling is seen in the far right column of Table 1.

The second criteria for setting the viscosity applies to finer resolution where nonlinearity in the momentum equation is sufficient to form an inertial boundary layer (which will be thinner than the frictional boundary layer of coarse-resolution models). In this regime, the role of the viscous terms is to dissipate grid-scale energy and noise. The required viscosity can be estimated by requiring the grid Reynolds number to be finite so that

$$A_2 \propto U_b \Delta \quad \text{or} \quad A_4 \propto U_b \Delta^3, \tag{116}$$

where U_b is the scale of the boundary speed, which itself is also a function of grid resolution. At very fine resolution, the grid-length characteristic timescale [equation (113)] of either form of viscosity becomes

$$\Delta t_{\max}^{A_{2,4}} \propto \frac{\Delta}{U_b}. \tag{117}$$

There is a marginal resolution where the viscous boundary layer is resolved, but the inertial boundary layer may be marginally resolved so that the maximum realized velocity is still a function of resolution. In this narrow regime, the characteristic timescale for viscosities becomes

$$\Delta t_{\max}^{A_{2,4}} \propto \frac{\Delta^2}{U_b L_b}, \tag{118}$$

where L_b is now the realistic inertial boundary layer scale. The three regimes for scaling behavior of the viscous limitation on maximum time step are listed in Table 1.

Figure 5 schematically shows the scaling of maximum time step discussed above and tabulated in Table 1. The absolute values are not necessarily appropriate to any specific model because discretization modifies the numerical coefficients that have been ignored for these curves. Of note, though, is that the scaling behavior of the largest stable time step allowed in a model is very complicated at coarse and marginal resolutions, more so than is indicated by the curves shown. In contrast, the scaling becomes simple at fine resolutions. In practice, the numerical details of the Laplacian and biharmonic friction operators will make the maximum allowed time step shorter. At coarse resolution, we typically find $\Delta t_{\max}^{A_4} < \Delta t_{\max}^{A_2} < \Delta t_{\max}^{u}$. This result is not apparent in Figure 5, as we have arbitrarily set all timescales to be equal at the grid scale. That is, at coarse resolution where the boundary currents are not resolved, the time step is usually limited by viscosity.

Besides grid-scale-dependent viscosities, which are now common in ocean models, *Smagorinsky* [1963, 1993] proposed that the Laplacian viscosity due to unresolved scales should be proportional to the resolved horizontal deformation rate times the squared grid spacing. In effect, the Smagorinsky viscosity tailors the local dissipation to both the local flow state and the local grid resolution using only a single non-dimensional adjustable parameter. If this parameter is properly chosen, the resulting viscosity ensures that the flow respects the numerical stability properties previously discussed even when simulating multiple flow and grid regimes such as occur in realistic ocean simulations. It is for these pragmatic reasons that the Smagorinsky viscosity has found notable use in large-scale ocean models [e.g., *Blumberg and Mellor*,

Table 1. Table of scaling relations for maximum time step permitted by each process.

Process	Timescale	$\Delta < L_b$	$\Delta > L_b$	
Advection, U $\Delta t_{\max}^{u} \propto$	$\dfrac{\Delta}{U}$	$U \sim U_b$ $\dfrac{\Delta}{U_b}$	$U \sim U_b L_b / \Delta$ $\dfrac{\Delta^2}{U_b L_b}$	
Gravity wave, C_g $\Delta t_{\max}^{c_g} \propto$	$\dfrac{\Delta}{c_g}$	$\dfrac{\Delta}{c_g}$		
Harmonic, $A_2 \propto$ $\Delta t_{\max}^{A_2} \propto$	$\dfrac{\Delta^2}{A_2}$	ΔU_b $\dfrac{\Delta}{U_b}$	$L_b U_b$ $\dfrac{\Delta^2}{U_b L_b}$	$\beta \Delta^3$ $\dfrac{1}{\beta \Delta}$
Biharmonic, $A_4 \propto$ $\Delta t_{\max}^{A_4} \propto$	$\dfrac{\Delta^4}{A_4}$	$\Delta^3 U_b$ $\dfrac{\Delta}{U_b}$	$L_b \Delta^2 U_b$ $\dfrac{\Delta^2}{U_b L_b}$	$\beta \Delta^5$ $\dfrac{1}{\beta \Delta}$

U is the flow speed realized in the model, U_b is maximum oceanic flow speed observed in boundary currents, c_g is the speed of the gravest internal gravity waves, Δ is the smallest grid spacing, L_b is a boundary layer scale, β is the planetary vorticity gradient at the Equator and A_2 and A_4 are the Laplacian and biharmonic viscosities, respectively.

1987; *Rosati and Miyakoda*, 1988; *Bleck and Boudra*, 1981; *Bleck et al.*, 1992], with *Griffies and Hallberg* [2000] also arguing for its utility with a biharmonic operator.

In Figure 5, we have also shown the Δt^f timescale arising from inertial oscillations. This timescale is independent of spatial resolution. The Δt^{c_g} timescale arises from internal gravity waves, and it has a scaling of Δ^1, with $c_g \sim NH$ invariant with resolution (Section 8.2). Vertical friction also has stability criteria, but is somewhat easier to treat implicitly in time because of the non-periodic nature of the vertical direction and the small aspect ratio of the computational grid. Notably, there are typically many fewer degrees of freedom in the vertical than the horizontal directions.

9. APPROXIMATIONS

We denote the set of equations developed thus far the unapproximated ocean equations. There have indeed been approximations made in deriving these equations: the fluid is approximated by a continuum, geopotentials are approximated by surfaces of constant oblate spheroid radius (Section 4.1), and the angular rotation rate of the Earth is assumed constant. Nonetheless, the suite of phenomena described by these equations is immense, with space scales and timescales ranging from millimeter and seconds to global and millenia. Various methods have been used to filter the equations to focus on particular subranges of this spectrum. From a modeling perspective, filtering, or approximating, the equations helps to reduce the cost of the resulting simulation. The previous discussion of linear modes anticipated some of the approximations commonly made in physical oceanography. We more formally review these approximations in this section.

9.1. Shallow Ocean Approximation

In the shallow ocean approximation,[12] the metric functions measuring horizontal distances on the Earth are dependent only on the lateral coordinates. Radial dependence of the metric functions is reduced to the constant radial factor $R = 6.367 \times 10^6$ m. This radius corresponds to the ellipsoid of best fit to the sea level geopotential. This is the appropriate value for the "Earth's radius" of use in ocean models. Note that R in ocean models is often taken as the slightly larger value $R = 6.371 \times 10^6$ m. This value corresponds to the radius of a sphere with the same volume as the Earth [*Gill*, 1982, page 597].

The shallow ocean approximation is motivated by noting the relatively small thickness of the ocean relative to the Earth's radius. Within this approximation, distances used to compute partial derivatives, covariant derivatives, areas, and volumes are determined by a metric tensor whose components are functions only of the lateral position on the sphere. Additionally, assumptions regarding the metric function dependence, as well as assumptions about the smallness of vertical accelerations associated with the hydrostatic approximation (Section 9.2), have implications toward the energy and angular momentum conservation laws. In particular, the angular momentum about the Earth's center is computed with a moment-arm that has a fixed radius $r = R$. Hence, motion in the vertical direction does not alter angular momentum in the shallow ocean approximation.

9.2. Hydrostatic Approximation

The hydrostatic approximation exploits the large disparity between horizontal motions, occurring over scales of many tens to hundreds of kilometers, and vertical motions, occurring over scales of tens to hundreds of meters. In this case, it is quite accurate to assume the moving fluid maintains the hydrostatic balance, whereby the vertical momentum equation takes the form

$$p_{,z} = -\rho \, g. \tag{119}$$

Because the vertical momentum budget has been reduced to the hydrostatic balance, the Coriolis force per mass must be given by

$$\mathbf{F}_c = -f \, \hat{\mathbf{z}} \wedge \mathbf{v}, \tag{120}$$

where

$$f = 2 \Omega \, \sin \phi \tag{121}$$

is the Coriolis parameter and ϕ is the latitude. That is, we drop the nonradial component of the Earth's angular rotation vector when computing the Coriolis force in a hydrostatic fluid.[13]

By truncating, or filtering, the vertical momentum budget to the inviscid hydrostatic balance, we are obliged to parameterize strong vertical motions occurring in convective regions, as hydrostatic equations cannot explicitly represent these motions. Such has led to various convective parameterizations in use by ocean models [*Killworth*, 1989; *Marshall and Schott*, 1999]. These parameterizations are essential for the models to accurately simulate various deep water formation processes, especially those occurring in the open ocean due to strong buoyancy fluxes.

The kinetic energy density for a hydrostatic fluid involves only the horizontal motions [e.g., *Bokhove*, 2000] so that

$$\mathcal{K} = \frac{1}{2}\mathbf{u} \cdot \mathbf{u}. \tag{122}$$

No other change is required for the energetic relations established in Section 6 to follow through for the hydrostatic fluid. This result is self-consistent with the scaling implicit in the hydrostatic balance that $w \ll |\mathbf{u}|$. Correspondingly, the hydrostatic relative vorticity vector is

$$\omega = \nabla \wedge \mathbf{u}, \tag{123}$$

where $\mathbf{u}$ is the horizontal velocity vector.

Making these three changes in the non-hydrostatic velocity equation (55) leads to the hydrostatic vector invariant velocity equation

$$[\partial_t + (f\hat{\mathbf{z}} + \omega) \wedge]\mathbf{v} = -\nabla \mathcal{E} + \rho^{-1}\nabla \cdot (\tau - \mathbf{I}p), \tag{124}$$

where, again, $\mathcal{E} = \mathbf{u} \cdot \mathbf{u}/2 + \Phi$. Note that the vertical component of equation (124) reduces to the hydrostatic balance upon setting the time derivative of the vertical velocity component to zero and by noting that the hydrostatic form of $\mathcal{K}$ and ω mean that $\nabla \mathcal{K} + \omega \wedge \mathbf{v}$ has a zero vertical component.

In hydrostatic ocean models, the effects of horizontal stresses are usefully split from vertical stresses when discussing friction. Friction from vertical stresses are generally parameterized by downgradient diffusion of momentum

$$(\nabla \cdot \tau)_{\text{vertical strain}} = \partial_z(\kappa_{\text{model}}\mathbf{u}_{,z}), \tag{125}$$

where $\kappa_{\text{model}} > 0$ is the vertical viscosity used in the model. The vertical (more generally dianeutral) viscosity is generally assumed to be equal to, or more often roughly ten times greater than, the vertical or dianeutral diffusivity employed for tracer. This vertical Prandtl number (ratio of viscosity to diffusivity) is not well measured in the ocean, leaving modelers to tune this parameter based on simulation integrity.

Vertically integrating the hydrostatic balance (119) over the full depth of the ocean fluid leads to

$$p_b - p_a = g \int_{-H}^{\eta} \rho \, dz, \tag{126}$$

with p_b the hydrostatic pressure at the ocean bottom and p_a the pressure at the ocean surface applied from the overlying atmosphere or ice. Use of this result in the mass budget (30) then leads to

$$\partial_t (p_b - p_a) = -\nabla \cdot \mathbf{U}^\rho + q_w \rho_w. \tag{127}$$

Assuming knowledge of the tendency for the applied surface pressure p_a, this budget is isomorphic to that for the Boussinesq surface height [equation (143)].

9.3. Oceanic Boussinesq Approximation

The Boussinesq approximation is an attempt to simplify the appearance of density in the ocean equations. In situ density in the large-scale ocean varies by a relatively small amount, with a 5% variation over the full ocean column at the upper end of the range, and most of this variation due to compressibility has no dynamical consequence. Furthermore, the dynamically relevent horizontal density variations, $\Delta\rho$, are on the order of 0.1%. Thus, it is justifiable to make approximations to the density in certain terms within the ocean equations, as discussed in this section.

There are two distinct steps to the Boussinesq approximation. We refer to these two steps in conjunction as the oceanic Boussinesq approximation. The first step of the Boussinesq approximation applies a linearization to the velocity equation (55) by removing the nonlinear product of density times velocity

$$[\partial_t + (f\hat{\mathbf{z}} + \omega)\wedge]\rho_o\mathbf{v} + \rho_o\nabla_z\mathcal{K} + \nabla_z p + \rho\nabla_z\Phi = \nabla \cdot \tau. \tag{128}$$

To obtain this equation, the product $\rho\mathbf{v}$ was replaced by $\rho_o\mathbf{v}$, where ρ_o is a constant Boussinesq reference density.[14] Importantly, one retains the in situ density dependence of the gravitational potential energy, and, correspondingly, it is retained for computing the hydrostatic pressure. It is through pressure that variations in density create critical dynamical effects. It is notable that as shown by equation (174), hydrostatic non-Boussinesq models based on pressure as the vertical coordinate naturally eliminate the nonlinear product $\rho\mathbf{v}$, thus removing the need to make any approximations [*Huang et al.*, 2001; *DeSzoeke and Samelson*, 2002; *Marshall et al.*, 2004; *Losch et al.*, 2004]. Interest in removing these nonlinear products arises in hydrostatic ocean modeling using depth-based vertical coordinates. The associated Boussinesq kinetic energy budget is given by

$$(\rho_o\mathcal{K})_{,t} + \nabla \cdot (\rho_o\mathcal{K}\mathbf{v} + p\mathbf{v} - \mathbf{v} \cdot \tau) = p\nabla \cdot \mathbf{v} - \rho\mathbf{v} \cdot \nabla\Phi - \rho_o\epsilon. \tag{129}$$

The second step in the oceanic Boussinesq approximation considers the mass continuity equation (5) where it is noted

that to leading order, the three-dimensional flow is incompressible

$$\nabla \cdot \mathbf{v} \approx 0. \tag{130}$$

It is this step in the approximation which filters acoustic modes, if they are not already filtered by the hydrostatic approximation (Section 8.1). More formally, the nearly incompressible observation manifests in the following scaling

$$\frac{\mathrm{d}\ln\rho}{\mathrm{d}t} \ll \nabla \cdot \mathbf{v}. \tag{131}$$

This scaling follows, as

$$\mathrm{d}\ln\rho/\mathrm{d}t \sim (U/L)\Delta\rho/\rho_o, \tag{132}$$

whereas each term of $\nabla \cdot \mathbf{v}$ scales as U/L or W/H. In this equation, (U,W) are horizontal and vertical velocity scales, and (L,H) are horizontal and vertical length scales. With $\nabla \cdot \mathbf{v} = 0$, mass conserving kinematics of the non-Boussinesq system are translated into volume conserving kinematics, in which case the mass of a parcel is approximated by $\mathrm{d}M = \rho_o\mathrm{d}V$, and the tracer mass in a parcel is approximated by $(\rho_o\mathrm{d}V)C$.

There are some confusing points that arise when considering the Boussinesq approximation. Namely, volume conservation for a parcel, through the mass budget (2), means that the three-dimensional velocity field $\mathbf{v}$ is non-divergent. A non-divergent velocity field cannot support acoustic modes (Section 8.1), and this is useful for purposes of large-scale modeling. A non-divergent velocity field also cannot support material evolution of in situ density [equation (3)]. Furthermore, through equation (61), a non-divergent velocity only supports, in general, adiabatic and isohaline motions. These motions are of interest for ideal incompressible fluid mechanics. They are, however, insufficient for describing the ocean circulation where mixing and heating are critical.[15]

How does the oceanic Boussinesq approximation work in ocean models? The oceanic Boussinesq approximation assumes the resolved flow to be incompressible, in which case acoustic modes are not supported. This approximation furthermore retains the dependence of density on pressure, heating, and salinity mixing, thus avoiding any assumption regarding the fluid properties. To support a nontrivial material evolution of density, as arises through pressure changes, mixing, and heating, requires a divergent velocity field, which is unresolved in oceanic Boussinesq models: the effect of this divergent velocity field manifests through non-trivial density evolution.

To illustrate how a Boussinesq model can support non-trivial density evolution, write the velocity as the sum of divergent and non-divergent components

$$\mathbf{v} = \mathbf{v}_{\mathrm{nd}} + \mathbf{v}_{\mathrm{d}}. \tag{133}$$

The divergent velocity $\mathbf{v}_{\mathrm{d}}$ is associated with the acoustic modes. Although we do not present a formal asymptotic analysis here, the acoustic fluctuations are of small amplitude and high frequency with respect to the oceanic flows of interest, which are embodied in $\mathbf{v}_{\mathrm{nd}}$. That is,

$$|\mathbf{v}_{\mathrm{d}}| \ll |\mathbf{v}_{\mathrm{nd}}|. \tag{134}$$

By construction, the continuity equation can now be split into the following two parts:

$$\nabla \cdot \mathbf{v}_{\mathrm{nd}} = 0 \tag{135}$$
$$\nabla \cdot \mathbf{v}_{\mathrm{d}} = -\mathrm{d}\ln\rho/\mathrm{d}t. \tag{136}$$

Given the scaling noted above, the non-divergent velocity contributes to leading order in the material time derivative on the right-hand side of equation (137) so that

$$\nabla \cdot \mathbf{v}_{\mathrm{d}} \approx -\frac{\mathrm{d}^{\mathrm{nd}}\ln\rho}{\mathrm{d}t}, \tag{137}$$

where $\mathrm{d}^{\mathrm{nd}}/\mathrm{d}t = \partial_t + \mathbf{v}^{\mathrm{nd}} \cdot \nabla$. The divergent velocity is seen, through mass conservation (3), to support a nonzero material evolution of density. This evolution, through equation (61), is affected by pressure fluctuations, salinity mixing, and heating

$$\frac{1}{\rho c_s^2}\frac{\mathrm{d}p}{\mathrm{d}t} + \beta_{\mathrm{S}}\frac{\mathrm{d}S}{\mathrm{d}t} - \alpha_\theta\frac{\mathrm{d}\theta}{\mathrm{d}t} = -\nabla \cdot \mathbf{v}_{\mathrm{d}}. \tag{138}$$

The oceanic Boussinesq approximation considers the resolved prognostic velocity field to be the non-divergent velocity $\mathbf{v}_{\mathrm{nd}}$, and this maintains an incompressible prognostic flow field that does not support acoustic modes. It is this velocity which is time stepped by using the Boussinesq momentum equation, and it is this velocity which transports tracer through advection. The divergent velocity $\mathbf{v}_{\mathrm{d}}$ does not vanish, however, as each term on the left-hand side of equation (138) is generally nonzero for the oceanic Boussinesq approximation. Instead, its divergence can, in principle, be diagnosed by evaluating the terms in equation (138).[16] Again, it is the existence of $\mathbf{v}_{\mathrm{d}}$ which allows the oceanic Boussinesq system to self-consistently employ a realistic equation of state in which density is a function of pressure, temperature, and salinity, thus supporting nonzero material time variations of the in situ density. These variations are critical for representing the thermohaline-induced variations in density which are key drivers of the large-scale ocean circulation.

9.3.1 Implications for gravitational potential energy. To obtain the gravitational potential energy equation, multiply the approximate mass budget in equation (137), involving the divergent velocity, by the geopotential Φ, to render the Boussinesq gravitational potential energy equation

$$(\rho\,\Phi)_{,t} + \nabla\cdot(\rho\,\Phi\,\mathbf{v}_{nd}) = \rho\,(\partial_t + \mathbf{v}_{nd}\cdot\nabla)\Phi - \Phi\rho\,\nabla\cdot\mathbf{v}_d.$$
(139)

Hence, from the perspective of the Boussinesq ocean model, which time steps the non-divergent velocity $\mathbf{v}_{nd}$, there is a new term affecting potential energy relative to the unapproximated budget (71). This term is given by

$$-\Phi\rho\,\nabla\cdot\mathbf{v}_d = \Phi\,\frac{d\rho}{dt}$$
(140)
$$= \Phi\rho\left(\frac{1}{\rho\,c_s^2}\frac{dp}{dt} + \beta_S\frac{dS}{dt} - \alpha_\theta\frac{d\theta}{dt}\right),$$
(141)

where we used equations (137) and (138) to replace the divergence $\nabla\cdot\mathbf{v}_d$ with the material changes in pressure, temperature, and salinity and where the material time derivative is taken with the resolved non-divergent velocity $\mathbf{v}_{nd}$. This source is affected by fluctuations in the pressure field, heating, and salinity mixing. Importantly, these three processes are coupled, with heating and mixing, for example, affecting pressure and pressure affecting dynamics. In Boussinesq models that replace the pressure dependence of density with depth dependence, as in equation (60), the source takes the form

$$-\Phi\rho\,\nabla\cdot\mathbf{v}_d = \Phi\rho\left(\frac{w}{\rho\,c_s^2}\frac{\partial\rho}{\partial p}\frac{\partial p_o}{\partial z} + \beta_S\frac{dS}{dt} - \alpha_\theta\frac{d\theta}{dt}\right).$$
(142)

Contrary to the more general form of equation (141), the pressure contribution is more readily diagnosed in an ocean model using this approximated equation of state. Further discussion of energetics of Boussinesq equations using the simpler equation of state can be found in *Vallis* [2006].

9.3.2 Implications for sea level height. We now ask how well the Boussinesq ocean model approximates the surface height relative to the non-Boussinesq model. The surface height in a Boussinesq ocean model satisfies the approximate balance of volume conservation for the column

$$\eta_{,t}^{\text{Bouss}} = -\nabla\cdot\mathbf{U} + q_w\rho_w/\rho_o,$$
(143)

where $\mathbf{U} = \int_{-H}^{\eta} dz\,\mathbf{u}$ is the vertically integrated horizontal velocity. This equation approximates the more exact result for

a mass conserving fluid which is obtained by vertically integrating the mass conservation equation (3) over a column of seawater, using the bottom kinematic boundary condition (24) and surface kinematic boundary condition (32), to find

$$\eta_{,t} = -\nabla\cdot\mathbf{U} + \frac{q_w\rho_w}{\rho(\eta)} - \int_{-H}^{\eta} dz\,\frac{d\ln\rho}{dt},$$
(144)

where $\rho(\eta)$ is the density at the ocean surface. The missing term in the Boussinesq surface height equation (143) arises from stretching and compressing a vertical column associated with changes in the ocean hydrography within a fluid column. The absence of this steric effect represents a limitation of Boussinesq ocean models for prognostically simulating, for example, effects of anthropogenic climate changes on sea level [*Greatbatch*, 1994; *Mellor and Ezer*, 1995].[17]

10. ELEMENTS OF VERTICAL COORDINATES

A key characteristic of rotating and stratified fluids, such as the ocean, is the dominance of lateral over vertical transport. Hence, it is traditional in ocean modeling to orient the two horizontal coordinates orthogonal to the local vertical direction as determined by gravity. The more difficult choice is how to specify the vertical coordinate and the associated transport across surfaces of constant vertical coordinate. Indeed, the choice of vertical coordinate is arguably the single most important aspect in the design of an ocean model. The main reason it is crucial is that practical issues of representation and parameterization are often directly linked to the vertical coordinate choice, and these issues enter at a level fundamental to developing the model algorithms.

10.1. Three Flow Regimes

Currently, there are three main vertical coordinates in use by ocean modelers, and they arose from applications focusing on complementary dynamical regimes. The following characterizes these regimes and provides a qualitative assessment of the abilities of the three coordinates. This assessment is subject to modifications due to algorithmic improvements, continually being developed, which push the envelope of applicability for the various vertical coordinates.

- *Upper ocean mixed layer.* This is a generally turbulent region dominated by transfers of momentum, heat, freshwater, and tracers with the overlying atmosphere, sea ice, rivers, etc. The mixed layer is of prime importance for climate system modeling and

operational oceanography. It is typically very well mixed in the vertical through three-dimensional turbulent processes. These processes involve non-hydrostatic physics, which requires very fine horizontal and vertical resolution (i.e., a vertical-to-horizontal grid aspect ratio near unity) to explicitly represent. In this region, it is useful to employ a vertical coordinate that facilitates the representation and parameterization of these highly turbulent processes. Geopotential and pressure coordinates, or their relatives, are the most commonly used coordinates, as they facilitate the use of very refined vertical grid spacing, which can be essential to simulate the strong exchanges between the ocean and atmosphere, rivers, and ice. These coordinates, in particular geopotential coordinates, have been the dominant choice of modelers focusing on global climate.

- *Ocean interior*. Tracer transport processes in the ocean interior predominantly occur along neutral directions [*McDougall*, 1987]. The transport is dominated by large-scale currents and mesoscale eddy fluctuations. Water mass properties in the interior thus tend to be preserved over large space scales and timescales (e.g., basin and century scales). It is critical to represent this property of the ocean interior in a numerical simulation of ocean climate. An isopycnal coordinate framework is well suited to this task, whereas geopotential and sigma models have problems associated with numerical truncation errors. As discussed by *Griffies et al.* [2000b], the problem can become more egregious as the model resolution is refined due to the enhanced levels of eddy activity that pumps tracer variance to the grid scale. Quasi-adiabatic dissipation of this variance is difficult to maintain in non-isopycnal models. We have more to say on this spurious mixing problem in Section 12.1.

- *Solid Earth boundary*. The solid Earth topography directly influences the ocean currents. In an unstratified ocean, the balanced flow generally follows lines of constant f/H, where f is the Coriolis parameter and H is the ocean depth. Additionally, there are several regions where density driven currents (overflows) and turbulent bottom boundary layer processes act as strong determinants of water mass characteristics. Many such processes are crucial for the formation of deep water properties in the World Ocean and for representing coastal processes in regional models. It is for this reason that terrain following sigma models have been developed over the past few decades, with their dominant application focused on the coastal and estuarine problem.

As reviewed by *Griffies et al.* [2000a], the geopotential, isopycnal, and sigma models each focus on one of the above regimes. Each do quite well within the confines of the separate regimes. It is in the overlap where problems arise. Because the ocean involves all of the regimes, there remain problems applying one particular coordinate choice for simulating the global ocean climate system. It is not clear whether these problems are insurmoutable. Indeed, much progress continues to be made at addressing various weaknesses. Nonetheless, the problems have motivated some effort to develop generalized vertical coordinates,[18] whereby the model algorithms determine the vertical coordinate according to the physical flow regime, e.g., pressure near the surface, isopycnal in the interior, and terrain following next to the solid Earth [*Bleck*, 2002]. We have more to say on such approaches when discussing solution methods in Section 11.

10.2. Depth and Pressure Isomorphism

A natural set of vertical coordinates of use for describing Boussinesq ocean models is based on the depth, or geopotential, vertical coordinate, as depth measures the volume per area above a point in a fluid column. Depth-based ocean models are the oldest of those models used for studying climate, with classical references for this first generation of ocean climate models being *Bryan and Cox* [1967]; *Bryan* [1969a, b]; *Bryan et al.* [1975]; *Bryan and Lewis* [1979]; *Cox* [1984]. The work of *Huang et al.* [2001], *DeSzoeke and Samelson* [2002], *Marshall et al.* [2004], *Losch et al.* [2004] highlights an isomorphism between depth-based Boussinesq mechanics and pressure-based non-Boussinesq mechanics (see Section 11.4 for details). This isomorphism has allowed for a straightforward evolution of depth-based models to the pressure-based models more commonly considered in recently developed ocean climate models. Pressure-based vertical coordinates are naturally used to describe non-Boussinesq hydrostatic fluids, as pressure in a hydrostatic fluid measures the mass per area above a point in a fluid column (Section 9.2).

10.3. Non-Orthogonality

The generalized vertical coordinates used in ocean modeling are not orthogonal, which contrasts with many other applications in mathematical physics.[19] Hence, it is useful to keep in mind the following properties that may seem odd on initial encounter.

The horizontal velocity in ocean models measures motions in the horizontal plane, perpendicular to the local gravitational field. That is, horizontal velocity is mathematically the same regardless the vertical coordinate, be it geopotential, isopycnal, pressure, or terrain following. The key motivation for maintaining the same horizontal velocity component is that the hydrostatic and geostrophic balances are dominant in the large-scale ocean. Use of an alternative quasi-horizontal velocity, for example one oriented parallel to the generalized surface, would lead to unacceptable numerical errors. Correspondingly, the vertical direction is anti-parallel to the gravitational force in all of the coordinate systems. We do not choose the alternative of a quasi-vertical direction oriented normal to the surface of a constant generalized vertical coordinate.

It is the method used to measure transport across the generalized vertical coordinate surfaces which differs between the vertical coordinate choices. That is, computation of the dia-surface velocity component detailed in Section 2.2 represents the fundamental distinction between the various coordinates. In some models, such as geopotential, pressure, and terrain following, this transport is typically diagnosed from volume or mass conservation. In other models, such as isopycnal layered models, this transport is prescribed based on assumptions about the physical processes producing a flux across the layer interfaces. We return to this key point in Section 11 when discussing solution methods.

11. SOLUTION METHODS

The purpose of this section is to introduce some of the steps needed to develop an algorithm for solving the ocean equations.

11.1. Finite Volumes

In formulating the budgets for an ocean model, it is typical to focus on mass, tracer, and momentum budgets for a finite domain or control volume, such as that of an ocean model grid cell. The budget for a grid cell is distinct from the budget for infinitesimal mass conserving Lagrangian fluid parcels moving with the fluid. Mass conserving fluid parcels form the fundamental system for which the budgets of mass, tracer, momentum, and energy are generally formulated from first principles. Grid cell budgets are then derived from the fundamental parcel budgets. Formulating budgets over finite-sized regions is an important first step toward developing a numerical algorithm. In particular, it is an essential step when working with a finite volume formulation [e.g., chapter 6 of *Hirsch*, 1988] such as with the MITgcm [*Marshall et al.*, 1997; *Adcroft et al.*, 1997].

The grid cells of concern for typical ocean models have vertical sides fixed in space–time, but with the top and bottom generally moving (Figure 6). In particular, the top and bottom either represent the ocean top, ocean bottom, or a surface of constant generalized vertical coordinate. As before, we assume that at no place in the fluid do the top or bottom surfaces of the grid cell become vertical. This assumption allows for a one-to-one relation to exist between geopotential depth z and a generalized vertical coordinate s (i.e., the relation is invertible).

To establish the grid cell budget, we integrate the budget for mass conserving fluid parcels over the cell volume. A first step is to take a differential relation of the form (7) and transform it to a finite domain relation by integrating over a region such as that for the grid cell shown in Figure 6. The following finite domain result follows by using standard vector calculus:
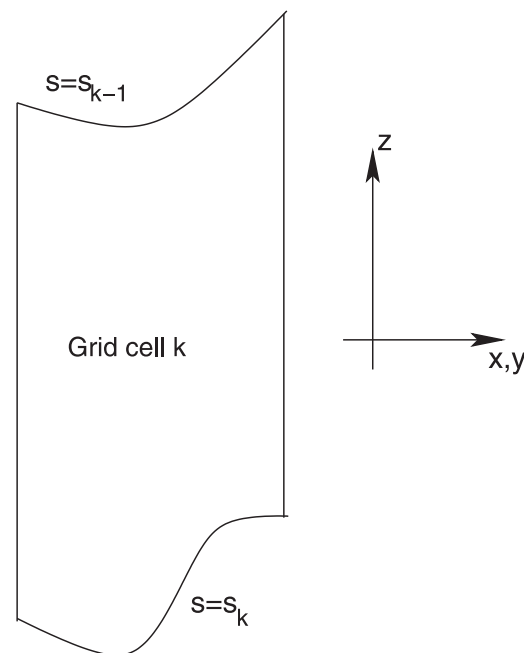

Figure 6. Schematic of an ocean grid cell labeled by the vertical integer k. Its sides are vertical and oriented according to $\hat{\mathbf{x}}$ and $\hat{\mathbf{y}}$, and its horizontal position is fixed in time. The top and bottom surfaces are determined by constant generalized vertical coordinates s_{k-1} and s_k, respectively. Furthermore, the top and bottom are assumed to always have an outward normal with a nonzero component in the vertical direction $\hat{\mathbf{z}}$. That is, the top and bottom are never vertical. We take the convention that the discrete vertical label k increases as moving downward in the column, and grid cell k is bounded at its upper face by $s = s_{k-1}$ and lower face by $s = s_k$.

$$\int \rho \frac{\mathrm{d}\Psi}{\mathrm{d}t}\,\mathrm{d}V = \partial_t \left(\int \rho\,\Psi\,\mathrm{d}V \right)$$
$$+ \int \mathrm{d}A_{(\hat{\mathbf{n}})}\,\hat{\mathbf{n}} \cdot (\mathbf{v} - \mathbf{v}^{(\mathrm{ref})})\,(\rho\,\Psi). \quad (145)$$

Hence, the mass weighted integral of the material time derivative of a field Ψ is given by the time derivative of the mass weighted field integrated over the domain, plus a boundary term that accounts for the transport across the domain boundaries, with allowance made for moving domain boundaries. Applying this result to the parcel tracer budget (33) leads to the finite domain tracer budget

$$\partial_t \left(\int C \rho\,\mathrm{d}V \right) = \int S^{(C)}\,\rho\,\mathrm{d}V$$
$$- \int \mathrm{d}A_{(\hat{\mathbf{n}})}\,\hat{\mathbf{n}} \cdot [(\mathbf{v} - \mathbf{v}^{\mathrm{ref}})\rho\,C + \mathbf{J}]. \quad (146)$$

Again, the left-hand side of this equation is the time tendency for tracer mass within the finite-sized grid cell region. When the tracer concentration is uniform, the SGS flux and source vanish, in which case the tracer budget (146) reduces to the finite domain mass budget

$$\partial_t \left(\int \rho\,\mathrm{d}V \right) = - \int \mathrm{d}A_{(\hat{\mathbf{n}})}\,\hat{\mathbf{n}} \cdot [(\mathbf{v} - \mathbf{v}^{\mathrm{ref}})\rho]. \quad (147)$$

Further work leads to similar domain statements for the momentum budget.

11.2. Reynolds Averaging

The finite volume budgets provide a first step along a particular avenue toward discretizing the ocean equations. The next step explicitly considers the shape and size of the grid cells, and approximates these geometric details as well as fields within these cells, given information resolved by the discrete model. This step exposes our lack of information about the scales smaller than the grid scale, and in so doing, introduces the SGS parameterization problem.

From the finite volume perspective, the SGS parameterization problem arises when a particular form of the resolved model variables is assumed, e.g., the model variables represent a mass weighted average of the continuous variables such as

$$\Psi_{\mathrm{model}} \equiv \frac{\int \Psi \rho\,\mathrm{d}V}{\int \rho\,\mathrm{d}V}. \quad (148)$$

The averaging described here is one form of a more generic Reynolds averaging procedure required to specify the ocean equations appropriate for the chosen discretization. Averaging of the form (148), or any other with more sophisticated weighting, introduces correlation terms between nonlinear products of SGS fields. A prescription for the correlations depends on the model grid and the unresolved physical processes. It also depends on whether the average is performed at a constant point in space (Eulerian average), on a moving surface such as an isopycnal (quasi-Lagrangian average), on a pressure surface, or another surface.

Regardless of the details of the Reynolds averaging, averaging over the subgrid scales appropriate for ocean models (e.g., scales smaller than 10 to 100 km) produces correlation terms that are many orders larger than the effects from molecular processes (e.g., molecular tracer diffusion and molecular friction). Hence, for all purposes of large-scale ocean modeling, the SGS flux $\mathbf{J}_c$ for tracer C is just that from Reynolds averaging, as is the momentum friction tensor τ.

Although we can, in principle, formulate a Reynolds averaging procedure for the ocean equations, there has not been a satisfying first principles closure for these equations relevant at the scale of global ocean models. Hence, the Reynolds averaged ocean equations are closed by introducing ad hoc steps that are unsatisfying both in principle and practice. We have more to say on this point regarding the lateral friction used in ocean models in Section 12.2.

11.3 General Comments on Solution Algorithms

The numerical procedures required to solve the ocean equations are dependent on details of the approximations or filters applied to the equations. For example, the non-Boussinesq and non-hydrostatic ocean equations,

$$[\partial_t + (2\mathbf{\Omega} + \boldsymbol{\omega}) \wedge\,]\mathbf{v} = -\nabla \mathcal{E} + \rho^{-1}\nabla \cdot (\tau - \mathbf{I}p) \quad (149)$$

$$\rho_{,t} + \nabla \cdot (\rho\,v) = 0 \quad (150)$$

$$(\rho\,\theta)_{,t} + \nabla \cdot (\rho\,\mathbf{v}\,\theta + \mathbf{J}_\theta) = \rho\,S_\theta \quad (151)$$

$$(\rho\,S)_{,t} + \nabla \cdot (\rho\,\mathbf{v}\,S + \mathbf{J}_S) = \rho\,S_S \quad (152)$$

$$\rho = \rho(\theta, S, p) \quad (153)$$

permit acoustics modes (Section 8.1; recall that $\mathcal{E} = \mathcal{K} + \Phi$ is the total mechanical energy per mass of a fluid parcel). An algorithm to solve these equations would significantly differ from an algorithm developed to solve the oceanic Boussinesq equations

$$[\,\partial_t + (2\,\Omega + \omega)\wedge\,]\rho_o\mathbf{v} = -\,\rho_o\nabla\mathcal{K} - \rho\nabla\Phi + \nabla\cdot(\tau - \mathbf{I}p)$$

$$(154)$$

$$\nabla\cdot\mathbf{v} = 0 \qquad (155)$$

$$\theta_{,t} + \nabla\cdot(\mathbf{v}\,\theta + \mathbf{F}_\theta) = S_\theta \qquad (156)$$

$$S_{,t} + \nabla\cdot(\mathbf{v}\,S + \mathbf{F}_S) = S_S \qquad (157)$$

$$\rho = \rho(\theta, S, p) \qquad (158)$$

which do not support acoustic modes. The choice of vertical coordinate also has a critical impact on the solution algorithm. The major distinction here is between Eulerian and Lagrangian viewpoints [*Adcroft and Hallberg*, 2006]. We briefly describe the procedures resulting from these two viewpoints for hydrostatic models, which can be applied to both the Boussinesq and non-Boussinesq momentum equations.

11.4. Sample Eulerian Algorithms

We start our consideration of solution algorithms with the Boussinesq hydrostatic equations written in geopotential (or depth) vertical coordinates. We also consider the shallow ocean approximation (Section 9.1). The resulting Boussinesq hydrostatic primitive equations are given by

$$[\partial_t + (f\,\hat{\mathbf{z}} + \boldsymbol{\omega})\wedge\,]\mathbf{v} + \nabla_z\mathcal{E} + \rho_o^{-1}\nabla_z p = \rho_o^{-1}\nabla\cdot\tau \quad (159)$$

$$\Phi_{,z} + \rho^{-1}p_{,z} = 0 \qquad (160)$$

$$\nabla_z\cdot\mathbf{u} + w_{,z} = 0 \qquad (161)$$

$$\theta_{,t} + \nabla_z\cdot(\mathbf{u}\,\theta) + (w\,\theta)_{,z} = S_\theta \qquad (162)$$

$$S_{,t} + \nabla_z\cdot(\mathbf{u}\,S) + (wS)_{,z} = S_s \qquad (163)$$

$$\rho = \rho(\theta, S, p). \qquad (164)$$

Notice that we allow for the general pressure dependence of the equation of state according to the discussion in Section 9.3. In these equations, ω, $\mathcal{E}$, and τ each assume their hydrostatic forms given in Section 9.2

$$\omega = \nabla\wedge\mathbf{u} \qquad (165)$$

$$\mathcal{E} = \mathbf{u}\cdot\mathbf{u}/2 + \Phi \qquad (166)$$

$$\nabla\cdot\tau = \partial_z(\kappa_{\text{model}}\mathbf{u}_{,z}) + \nabla\cdot\tau_{\text{horizontal strain}}. \qquad (167)$$

Equations (159)–(164) are seven equations with seven unknowns (u, v, w, p, θ, S, ρ). There are four predictive or prognostic equations: two components of the horizontal velocity equation (159) and the potential temperature and salinity equations (162) and (163). There are three diagnostic equations: the hydrostatic balance (160), the Boussinesq continuity equation (161), and the equation of state (164). Predictive equations are used to update in time (i.e., predict) the corresponding model variable, while the remaining variables are determined by the diagnostic relations.

The system of equations (159)–(164) can be solved using explicit-in-time algorithms. For example, given an initial hydrographic specification of θ and S and p, we can proceed as follows:

1. The in situ density ρ can be diagnosed from the equation of state (164) using pressure at a lagged time step [e.g., *Dewar et al.*, 1998; *Griffies et al.*, 2001];
2. Hydrostatic pressure p can be diagnosed by vertical integration of the hydrostatic equation (160);
3. Horizontal velocity **u** can be predicted using the velocity equation (159);
4. The vertical velocity component w can be diagnosed by vertical integration of the continuity equation (161);
5. Tracers θ and S can be predicted using the tracer equations (162) and (163);
6. Returning to step 1 repeats the cycle for a subsequent time step.

This algorithm will work using fully explicit time-integration methods. However, the time step will be limited by the fastest mode, which, in this case, is the external gravity wave which can exceed speeds of 200 ms^{-1} in the deep ocean. As noted in Section 8.2, resolving external gravity waves in a global ocean model is prohibitively expensive. An alternative treatment of the fast external modes is discussed in Section 11.6.

The hydrostatic Boussinesq equations (159)–(164) permit four linear internal modes of variability: two inertia–gravity, one geostrophic, and one thermohaline mode.[20] Furthermore, the equations are written in a transparent form for developing solution algorithms, as there is no ambiguity about the way to use each equation, and there is only one obvious candidate for which predictive equation to use to predict a particular variable. As we now discuss, changing the nature of an equation within the system can potentially lead to inconsistencies. To illustrate this point, consider the non-Boussinesq and hydrostatic primitive equations written with a general vertical coordinate s:

$$[\partial_t + (f\hat{\mathbf{z}} + \boldsymbol{\omega})\wedge]\mathbf{v} + \nabla_s \mathcal{E} + \rho^{-1}\nabla_s p = \rho^{-1}\nabla \cdot \boldsymbol{\tau} \quad (168)$$

$$\partial_s \Phi + \rho^{-1}\partial_s p = 0 \qquad (169)$$

$$(\rho\, z_{,s})_{,t} + \nabla_s \cdot (\rho\, \mathbf{u}\, z_{,s}) + (\rho\, w^{(s)})_{,s} = 0 \qquad (170)$$

$$(\rho\, z_{,s}\, \theta)_{,t} + \nabla_s \cdot (\rho\, \mathbf{u}\, z_{,s}\, \theta) + (\rho\, w^{(s)}\, \theta)_{,s} = \rho\, z_{,s} S_\theta \qquad (171)$$

$$(\rho\, z_{,s}\, S)_{,t} + \nabla_s \cdot (\rho\, \mathbf{u}\, z_{,s}\, S) + (\rho\, w^{(s)}\, S)_{,s} = \rho\, z_{,s} S_S \qquad (172)$$

$$\rho = \rho(\theta, S, p)$$
$$(173)$$

where, again, $w^{(s)} = z_{,s}\, \mathrm{d}s/\mathrm{d}t$ is the dia-surface velocity component introduced in Section 2.2. Equations (168)–(173) also permit four linear internal modes of variability, but the equations now contain five time derivatives. Hence, there are now five predictive equations and only two diagnostic relations. Consider a situation where $z_{,s}$ is known or prescribed (for instance, with geopotential vertical coordinates $z_{,s} = 1$); there are then two possible equations that might be used to determine the in situ density ρ: either equation (170) or equation (173). It is not immediately obvious which is the proper equation to use. If we use the equation of state (173), then mass conservation (170) might be violated, but if we use mass conservation, then the equation of state may not be satisfied. A judicious choice of vertical coordinate removes this ambiguity. For example, setting $s = p$ and noting that $g\rho z_{,p} = -1$ brings equations (168)–(173) into the form

$$[\partial_t + (f\hat{\mathbf{z}} + \boldsymbol{\omega})\wedge]\mathbf{u} + \nabla_p \mathcal{E} = \rho^{-1}\nabla \cdot \boldsymbol{\tau} \qquad (174)$$

$$\partial_p \Phi + \rho^{-1} = 0 \qquad (175)$$

$$\nabla_p \cdot \mathbf{u} + \partial_p(\dot{p}) = 0 \qquad (176)$$

$$\theta_{,t} + \nabla_p \cdot (\mathbf{u}\, \theta) + (\theta\, \dot{p})_{,p} = S_\theta \qquad (177)$$

$$S_{,t} + \nabla_p \cdot (\mathbf{u}\, S) + (S\, \dot{p})_{,p} = S_S \qquad (178)$$

$$\rho = \rho(\theta, s, p), \qquad (179)$$

where $\dot{p} = \mathrm{d}p/\mathrm{d}t$ is the material time derivative of pressure. These equations are, term for term, isomorphic to the Boussinesq hydrostatic geopotential coordinate equations (159)–(164). This isomorphism, already mentioned in Section 10.2, has been exploited in meteorology for many years [e.g., *Haltiner and Williams*, 1980] and more recently has been brought into use for non-Boussinesq ocean models [*Huang et al.*, 2001; *DeSzoeke and Samelson*, 2002; *Marshall et al.*, 2004; *Losch et al.*, 2004]. A solution procedure for the compressible pressure-coordinate equations (174)–(179) is identical to that for the incompressible equations in height coordinates (159)–(164), except solving for Φ instead of p

and without the need to temporally lag pressure to evaluate the equation of state.

Returning to the general coordinate non-Boussinesq ocean equations (168)–(173), we note that there are two distinct approaches to solving these equations. The approaches are distinguishable by their treatment of the continuity equation (170). The first method adopts an Eulerian perspective, used in the preceding algorithms, where continuity is used to diagnostically determine transport across coordinate surfaces (vertically integrating equation (170) for the dia-surface velocity component $w^{(s)}$). To achieve this, the time derivative $(\rho z_{,s})_{,t}$ must be prescribed, or more specifically, $\rho z_{,s}$ must be functionally related to other dependent or independent model variables. This is the case for the terrain-following coordinates commonly referred to as σ-coordinates of which a simple example is the *Phillips* [1957] sigma-coordinate $s = \sigma = (p - p_a)/(p_b - p_a)$, where p_b is the pressure at the solid-Earth boundary, and p_a is the pressure applied at the top of the water column. For this vertical coordinate, the factor $\rho z_{,s} = -(p_b - p_a)/g$ is minus the mass per area of the water column, and this two dimensional field is predicted by the external mode equations (Section 11.6).

11.5. Sample Lagrangian Algorithms

The second approach to solving the non-Boussinesq ocean equations (168)–(173) adopts the Lagrangian perspective, common to most layer (isopycnal or stacked shallow water) models. For this approach, the cross-coordinate flow, $w^{(s)}$, is prescribed. We focus here on isopycnal models, in which case $w^{(s)}$ is set to zero in the adiabatic limit. The continuity equation (170) is then used prognostically to predict the layer mass per area

$$\rho\, \mathrm{d}z = \rho\, z_{,s}\, \mathrm{d}s. \qquad (180)$$

Most isopycnal algorithms [e.g., *Bleck et al.*, 1992] assume the potential density of each layer to be constant in time and space. With zero dia-surface flow, the continuity equation (170) leads to

$$(\rho\, z_{,s})_{,t} + \nabla_s \cdot (\rho\, \mathbf{u}\, z_{,s}) = 0, \qquad (181)$$

which predicts layer mass per area. A difficulty with this approach is that θ and S are predicted independently. Hence, there is no guarantee that the diagnosed potential density $\rho_{ref} = \rho(\theta, S, p_{ref})$ will correspond to the assumed potential density of the layer. There are various approaches to correcting for this evolution of layer density, such as wrapping the layer remapping together with dianeutral processes like cabelling, as proposed by *Oberhuber* [1993], *McDougall and Dewar*

[1997], *Hallberg* [2000]. We have more to say on this point in Section 12.1.

A more general approach has been proposed [*Hirt et al.*, 1974; *Bleck*, 2002] in which remapping is used to reallocate mass so as to bring the layer densities back to their targets. This extra step is the foundation of the arbitrary Lagrangian–Eulerian method (ALE), which allows for the remapping step to remap to any coordinate, not necessarily isopycnal. The ALE method has become the preferred approach for general coordinate modeling because it is quite flexible. The ALE-based procedure for solving the general-coordinate hydrostatic non-Boussinesq equations is generally as follows:

1. Given the mass per area $\rho z_{,s} ds$ of a layer, pressure can be found by vertically integrating the hydrostatic equation (169).
2. Given the pressure p, potential temperature θ, salinity S, the in situ density can be calculated from the equation of state (173).
3. The horizontal velocity $\mathbf{u}$ can be predicted using the velocity equation (168).
4. The mass thickness $\rho z_{,s} ds$, θ, and S can be predicted, assuming the generalized s surfaces are material ($\dot{s} = 0$), by using equations (170)–(172).
5. A remapping step redistributes mass, θ, and S so as to bring the surfaces of s to the desired position. This step introduces irreversible numerical mixing processes (Section 12.1), although it is sometimes hidden within the operators describing physical mixing processes [*Hallberg*, 2000].

11.6. Solving for the External Mode

The ocean external modes are significantly faster than the internal modes. Treating the full three-dimensional system explicitly with a time step short enough to resolve external motions would be prohibitively expensive. There are three methods that have been used for avoiding this limitation: the rigid lid method, the split-explicit method, and the time-implicit method.

Ocean model algorithms approximate the external mode by using solutions to the vertically integrated continuity and momentum equations. These equations are coordinate-independent and take the form

$$\partial_t \mathbf{U}^\rho + g(H + \eta)\nabla p_b + \mathbf{F}(\mathbf{U}^\rho) = \mathbf{S} \qquad (182)$$

$$\partial_t p_b + \nabla \cdot \mathbf{U}^\rho = q_w \rho_w + \partial_t p_a \qquad (183)$$

where $\mathbf{U}^\rho = \int_{-H}^{\eta} \rho \mathbf{u} dz$ [equation (31)] was introduced when discussing mass conservation for a vertical column. We have grouped various terms into fast ($\mathbf{F}$) and slow ($\mathbf{S}$) vectors. The choice of which terms are placed in the fast vector ($\mathbf{F}$) is a matter of taste, and it varies from model to model. For the present discussion, we ignore these terms, yet note that many models include the Coriolis force in this vector, whereas others also include horizontal friction or bottom drag. The linear forms of equations (182) and (183) describe plane waves with phase and group speed of $c_g \sim \sqrt{gH}$. These are the external gravity waves discussed in Section 8.2. The essential role of these equations is to allow the external mode to adjust the system to an imbalance of divergent mass transport. This adjustment occurs on timescales that are short compared to the baroclinic evolution of the model.

The first generation of ocean climate models, based on the algorithm of *Bryan* [1969a], employed the rigid lid approximation with the oceanic Boussinesq approximation. This approach sets the time tendency of the surface height in equation (143) to zero and drops the surface water fluxes. Consequently, the vertically integrated horizontal velocity is non-divergent, thus allowing for the introduction of a streamfunction for the vertically integrated velocity in the solution algorithm. This approach was revolutionary for its time, as it facilitated efficient time stepping, whereby fast barotropic gravity waves are absent from the algorithm. Nonetheless, it is physically unsatisfying due to the inability to represent tides and through the lack of a direct water forcing [*Huang*, 1993]. Additionally, it is computationally awkward, as the resulting elliptic problem is very difficult to solve accurately in realistic ocean geometries. Hence, practitioners often halted the elliptic solver searches after a maximum number of steps regardless of the remaining distance to convergence.

The split-explicit approach solves the depth averaged equations explicitly with a short external mode time step. In contrast, the baroclinic portion of the model is time stepped with a larger time step determined by the slower baroclinic processes. Investigations have revealed that the split-explicit methods, such as those from *Blumberg and Mellor* [1987], *Bleck and Smith* [1990], *Killworth et al.* [1991], *Dukowicz and Smith* [1994], *Griffies et al.* [2001], can be just as efficient computationally as the rigid lid method, yet without sacrificing tides, direct surface water forcing, or compromising the realism of the ocean geometry. Hence, the rigid lid methods are largely obsolete in the more recent (e.g., post-2000) models used for global climate.

There are many variants on the implementation details of the split-explicit approach, with essentially two broad strategies taken. In Eulerian models, the flow is partitioned as

$$\mathbf{u} = \hat{\mathbf{u}} + \bar{\mathbf{u}}, \qquad (184)$$

with the barotropic component determined by the following depth and mass-weighted average:

$$\bar{\mathbf{u}} = \frac{\mathbf{U}^\rho}{\displaystyle\int_{-H}^{\eta} \rho\, \mathrm{d}z}. \qquad (185)$$

The baraclinic component is the remainder: $\hat{\mathbf{u}} = \mathbf{u} - \bar{\mathbf{u}}$. The full momentum equations may be rewritten to predict only the baroclinic component in a manner analogous to the rigid lid approach of *Bryan* [1969a; e.g., *Blumberg and Mellor*, 1987; *Killworth et al.*, 1991; *Griffies et al.*, 2001]. Alternatively, the full flow may be corrected by replacing the barotropic component with the results of the barotropic solver. In Lagrangian vertical coordinate models, the nonlinearity of the continuity equation and, in particular, the nonlinearity of the advection schemes used to guarantee positive definiteness of thickness, make a decomposition of the flow according to equation (184) troublesome. The alternative approach used is to make adjustments to either the layer transports or the barotropic transports to make them consistent [e.g., *Bleck and Smith*, 1990]. Earlier models allowed these two estimates of barotropic transport to remain inconsistent and used weak coupling to drive one toward the other [*Hallberg*, 1997; *Higdon*, 2005].

The time-implicit treatment of the external mode requires that the fast barotropic terms, principally the pressure gradient force due to the bottom pressure and the depth-integrated mass divergence, to be evaluated in the future part of the time step (i.e., solved implicitly). The analogous depth average equations can be rearranged into a two-dimensional elliptic equation which closely resembles the wave equation in structure. This wave equation takes the form

$$\left[\nabla \cdot ((H + \eta)\nabla) - \frac{\Gamma}{\Delta t^2} \right] p_b^{n+1} = \text{r.h.s.} \qquad (186)$$

where the details of the right-hand side terms (r.h.s.) and Γ are dependent on the choice of time discretization. Notably, this elliptic operator is better conditioned than that arising in the rigid lid approach [*Dukowicz and Smith*, 1994], and so convergence is more rapid. Such is fortunate, as this elliptic equation must be solved fairly accurately to ensure that the residual mass divergence does not grow during the integration of the baroclinic model. The elliptic equation should strictly be nonlinear. However, it is typically linearized by lagging the nonlinear terms in time. For deep ocean calculations, this linearization is justifiable, but it becomes less appropriate in shallow regions. The time-implicit approach can

recover the rigid lid approximation by dropping the Helmholtz term ($\Gamma/\Delta t^2 \to 0$). The physical interpretation of this limit is that we are finding p_b so as to adjust the barotropic flow to be exactly non-divergent.

11.7. Non-Hydrostatic Methods

Non-hydrostatic effects are significant only for large aspect ratio flows (e.g., Kelvin–Helmholtz instability) but can lead to systematic differences at small aspect ratios. Non-hydrostatic global models generally are too expensive to be in routine use. However, as spatial resolution is refined and the sub-mesoscale is resolved, non-hydrostatic effects need to be included. Relaxing the hydrostatic approximation in the non-Boussinesq equations permits acoustic modes, and so most non-hydrostatic models of the ocean assume the oceanic Boussinesq approximation. The methods of *McDougall et al.* [2003] might well be able to incorporate quasi non-Boussinesq effects in non-hydrostatic models.

The non-hydrostatic algorithms used in ocean models use derivatives of the projection method [*Chorin*, 1968]. Here, the problem is posed as follows: what (non-hydrostatic) pressure gradients are required to correct the flow to make the flow exactly non-divergent? By summarizing the full three-dimensional momentum equations and continuity as

$$\rho_o \mathbf{v}^{n+1} + \Delta t \nabla p = \rho_o \mathbf{v}^n + \Delta t\, G \qquad (187)$$

$$\nabla \cdot \mathbf{v}^{n+1} = 0 \qquad (188)$$

where $\mathbf{G}$ is the vector of all explicit forces, a rearrangement and substitution of variables yields the three-dimensional elliptic equation

$$\nabla \cdot \nabla p = \nabla \cdot \left(\frac{\rho_o}{\Delta t} \mathbf{v}^n \right) + \nabla \cdot \mathbf{G}. \qquad (189)$$

The first term on the right-hand side is important for implementation; otherwise, a residual divergence in the system may accumulate and lead to numerical instability. The three-dimensional elliptic equation for pressure replaces the vertical integration for hydrostatic pressure in the hydrostatic algorithms discussed in Section 9.2.

In the atmosphere, non-hydrostatic models do not make the Boussinesq approximation, and such models therefore permit acoustic modes. However, atmospheric acoustic waves are slow enough to be resolvable explicitly in the horizontal directions, whereas an implicit treatment in the vertical direction is sufficient to render a stable algorithm. Thus, non-hydrostatic atmospheric models are essentially hyperbolic, while oceanic non-hydrostaic models are elliptic in pressure.

12. SUMMARY AND OUTSTANDING PROBLEMS

We have aimed in this chapter to present a compendium of the scientific rationale for the equations used in physical ocean models. This rationale is independent of model resolution, and so provides a basis for both coarse-resolution global models as well as very fine-resolution regional and coastal models. Differences in applications largely reflect on the approximations made to the equations as well as choices for SGS parameterizations.

There remain many outstanding problems with ocean models. A large number can be alleviated by refining the resolution, thus allowing the simulation to rely less on the often ad hoc SGS parameterizations and depending more on resolved dynamical features. This reliance on enhanced resolution has a cost in computational expense. It also is limited by numerical algorithmic integrity. Namely, for enhanced resolution to accurately capture the dynamics, the numerical methods must respect the dynamics. This statement is relevant at all resolutions. However, large levels of viscous dissipation generally used at coarse resolution can sometimes hide problems revealed only upon refining the grid and reducing viscosity. Our goal in this final section is to discuss two issues which present a limitation on ocean simulations and which do not appear to be remedied upon refining the resolution: (a) the spurious mixing problem and (b) the specification of horizontal friction.

12.1. The Spurious Mixing Problem

Direct measurements of tracer diffusivity in the ocean were pioneered with the purposeful passive tracer release experiments of *Ledwell et al.* [1993]. These measurements indicate that on the large scales (on the order of hundreds of kilometers), the associated neutral to dianeutral anisotropy in mixing can be as high as 10^8 in the ocean interior, with smaller anisotropies in regions of strong dianeutral mixing such as within boundary layers or above rough topography. Another method for determining the dianeutral diffusivity uses the indirect approach suggested by *Osborn* [1980] and reviewed by *Gregg* [1987] and *Davis* [1994]. In this indirect approach, momentum dissipation at small scales is directly measured, and dianeutral diffusivity is inferred based on a theoretical connection between buoyancy mixing and momentum dissipation. These microstructure techniques likewise indicate that the levels of interior dissipation are very small, in general agreement with the direct tracer release measurements. They each indicate that the level of interior dianeutral mixing corresponds to a diffusivity on the order $10^{-5}\,\mathrm{m^2 s^{-1}}$, with 10 to 100 times smaller values suggested at the equator by measurements from *Gregg et al.* [2003]. This

is a strong statement regarding the level to which the ocean interior respects the neutral orientation of transport. Ocean models, especially those used for purposes of climate simulations, must respect this anisotropy.

For a numerical simulation to respect these small levels of mixing requires a tremendous level of integrity for the tracer transport algorithms. There are two main approaches that modelers have taken in this regard. First, modelers intent on respecting this level of mixing have tended to work with an isopycnal vertical coordinate. The advantage isopycnal models have over alternative vertical coordinates is that their advective transport operator is the sum of a two-dimensional lateral operator which acts independently of the dia-surface transport operator, with the dia-surface transport set, ideally, according to physical processes leading to mixing between density classes. Although suitable for the ideal adiabatic simulations, this is not sufficient for the real ocean. Here, a nonlinear equation of state introduces new physical sources of mixing, and the independent transport of two active tracers (temperature and salinity) requires remapping algorithms to retain fields within pre-specified density classes. These details introduce levels of dianeutral mixing which have yet to be systematically documented. They have nonetheless generally been considered negligible, with remapping often wrapped together with diapycnal processes [*Oberhuber*, 1993; *McDougall and Dewar*, 1997; *Hallberg*, 2000], thus using physical mixing processes in lieu of numerical mixing.

The second approach focuses on improving numerical transport methods. As discussed in *Griffies et al.* [2000b], the difficulties of maintaining small levels of spurious mixing are enhanced when moving to an eddying regime where the quasi-geostrophic cascade pumps tracer variance toward the grid scale. Dissipating this variance is required to damp unphysical grid scale features. Dissipation methods include the addition of an operator acting on the small scales (e.g., Laplacian or biharmonic), or dissipation inherent in the advection scheme (e.g., odd order schemes and/or flux limiters). However, most dissipation methods remain ignorant of the constraints based on spurious dianeutral transport. Notable exceptions include the adiabatic dissipation arising from the Laplacian operator of *Gent and McWilliams* [1990] and *Gent et al.* [1995], which attempts to parameterize physical processes, or the operators of *Smith* and *Gent* [2004] and *Roberts and Marshall* [1998], which are motivated from numerical considerations. For advection operators and dissipation operators, the question remains whether they can be constructed so that in practice, their numerical truncation errors are comparable with, or ideally less than, the tiny levels of physical mixing seen in the ocean interior. This problem remains at the forefront of ocean modeling practice, especially as eddying simulations for global climate become the norm.

12.2. Frictional Stresses in Ocean Models

As discussed in Section 8.4, modelers generally must set the strength of lateral fricional stresses to satisfy requirements of certain numerical constraints.[21] For example, in the presence of solid-Earth boundaries, friction must be sufficient to maintain a nontrivial side boundary layer. Even in the absence of boundaries, horizontal friction must be sufficient to maintain a finite grid Reynolds number $U\Delta/\nu_{\mathrm{model}}$, with ν_{model} the model horizontal viscosity. Otherwise, the simulation may go unstable, or at best, it will produce unphysical noise-like features. This constraint on the numerical simulation is unfortunate, as it generally requires a model viscosity many orders of magnitude larger than the molecular viscosity relevant for the ocean. The reason is that model grid sizes, even in mesoscale eddy-permitting simulations, are much larger than the Kolmogorov scale ($\approx 10^{-3}$m) where molecular friction acts.

Various methods have been engineered to employ the minimal level of horizontal friction required to meet the numerical constraints [e.g., *Griffies and Hallberg*, 2000; *Large et al.*, 2001; *Smith and McWilliams*, 2003]. Notably, modelers generally assume that the frictional stresses are isotropic in the horizontal direction, with anisotropy only between the horizontal and vertical stresses. However, as noted by *Large et al.* [2001] and *Smith and McWilliams* [2003], we may choose to allow one more degree of freedom by breaking horizontal isotropy. Doing so provides a practical avenue toward reducing the overall dissipation, and it can have a nontrivial advantage for simulating certain features such as the equatorial currents.

Quite generally, methods for selecting model horizontal friction are ad hoc. They furthermore lead to some of the most unsatisfying elements in ocean model practice, as details of friction can strongly influence the simulation. Unfortunately, it appears that this sensitivity remains as resolution is refined [*Chassignet and Garraffo*, 2001]. One compelling approach to resolve this problem with ad hoc friction operators is to remove horizontal friction operators from the models altogether. In their place, one allows dissipation to occur within the momentum transport operators. This approach, formally termed implicit large eddy simulation, holds some promise [*Margolin et al.,* 2006]. It is analogous to the trend for handling the tracer equation in eddying simulations, whereby lateral SGS operators are removed or rendered far subdominant to the resolved advection process. The hope is that numerical methods for the resolved transport can be designed that are smarter and more robust than the suite of SGS operators engineered thus far.

Notes

1. The three dimensional velocity vector is written $v = (u, w)$, with $u = (u, v)$ the horizontal components and w the vertical component.
2. This notation is standard in theoretical physics. It serves our purposes by distinguishing between a partial derivative and a tensor label.
3. Water crossing the ocean surface is typically quite fresh, such as for precipitation or evaporation. However, rivers and ice melt can generally contain a nonzero salinity.
4. We assume there to be no mass flux through the solid Earth boundary.
5. Electromagnetic effects are generally ignored in physical ocean models.
6. Note that $\mathrm{Wkg^{-1}} = \mathrm{m^2 s^{-3}}$.
7. For spherical coordinates, r is the radial position, λ is the longitude, and ϕ is the latitude.
8. We consider seawater to be a binary system of fresh water and salt. The factor of 1000 accounts for the use of salinity in parts per thousand rather than salt concentration.
9. This meaning for isentropic ocean models is consistent with the models not including frictional heating.
10. Note that when $\epsilon_{\mathrm{nh}} = 0$, we require the buoyancy force to recover hydrostatic balance. We ignore this force here to focus on the linear dynamical modes arising without buoyancy.
11. As noted by *Griffies et al.* [2000b], it is prudent to admit at least two grid points in a Munk boundary layer to minimize spurious levels of mixing associated with advection truncation errors.
12. This approximation is distinct from the shallow water approximation.
13. The quasi-hydrostatic approximation discussed in *Marshall et al.* [1997] keeps the full Coriolis terms, but still integrates a balance equation for pressure as in Section 11.4.
14. Some ocean models choose the Boussinesq density to be $\rho_o = 1000\mathrm{kg\ m^{-3}}$ [e.g., *Cox*, 1984], which is roughly the density of freshwater at standard conditions, whereas others [e.g., *Griffies et al.*, 2004] choose $\rho_0 = 1035\mathrm{kg\ m^{-3}}$, which is roughly the mean density of seawater in the World Ocean [page 47 of *Gill*, 1982].
15. See *Veronis* [1973] for a thorough discussion, with critique, of the Boussinesq approximation in which salinity, temperature, and potential density are materially conserved.
16. The existence of a nonzero v_{d} in the oceanic Boussinesq approximation is analogous to the presence of a nonzero ageostrophic flow in quasi-geostrophic models in which the ageostrophic flow is not directly computed but can be diagnosed.
17. For diagnostic purposes in a non-Boussinesq model, it is of interest to determine the local effects from column stretching on sea level. The material time derivative in equation (144) is difficult to diagnose. Hence, we offer the alternative expression, derived from the column integrated mass budget (30): $\eta_{,t} = (1/\bar{\rho})(-\nabla \cdot \mathbf{U}^\rho + q_{\mathrm{w}}\rho_{\mathrm{w}} - D\partial_t \ln\bar{\rho})$, with $\bar{\rho} = (H + \eta)^{-1}\int_{-H}^{\eta} \mathrm{d}z\rho$ the vertically averaged density in a column. It is now clear that $-D\partial_t \ln \bar{\rho}$ represents a positive contribution to the surface height when the vertically averaged in situ density within a column decreases.

18. So far as we know, generalized vertical coordinates are synonymous with hybrid vertical coordinates.

19. It is nonetheless notable that a similar set of generalized vertical coordinates has found use in other areas of theoretical physics. In particular, condensed matter physicists and biophysicists studying the dynamics of fluctuating membranes use these coordinates, where the coordinates go by the name Monge gauge. Their mathematical aspects are lucidly described in Section 10.4 of *Chaikin and Lubensky* [1995].

20. See *Müller and J. Willebrand* [1986] for a discussion of a thermohaline mode arising from the presence of two tracers, temperature and salinity, affecting in situ density.

21. There is a notable exception to the discussion here, where *Holloway* [1992] argues that unresolved stresses associated with interactions between the ocean and the solid-Earth boundary impart a net momentum to the fluid.

REFERENCES

Adcroft, A., and R. W. Hallberg (2006), On methods for solving the oceanic equations of motion in generalized vertical coordinates, *Ocean Model.*, *11*, 224–233.

Adcroft, A., C. Hill, and J. Marshall (1997), Representation of topography by shaved cells in a height coordinate ocean model, *Mon. Weather Rev.*, *125*, 2293–2315.

Adcroft, A., C. Hill, and J. Marshall (1999), A new treatment of the Coriolis terms in c-grid models at both high and low resolutions, *Mon. Weather Rev.*, *127*, 1928–1936.

Apel, J. R. (1987), *Principles of Ocean Physics*, International Geophysics Series, vol. 38, Academic Press, London.

Arakawa, A. (1966), Computational design for long-term numerical integration of the equations of fluid motion: Two-dimensional incompressible flow. Part 1, *J. Comput. Phys.*, *1*, 119–143.

Arakawa, A., and Y.-J. Hsu (1990), Energy conserving and potential enstrophy dissipating schemes for the shallow water equations, *Mon. Weather Rev.*, *118*, 1960–1969.

Arakawa, A., and V. Lamb (1981), A potential enstrophy and energy conserving scheme for the shallow water equations, *Mon. Weather Rev.*, *109*, 18–36.

Aris, R. (1962), *Vectors, Tensors and the Basic Equations of Fluid Mechanics*, Dover Publishing, New York.

Bacon, S., and N. P. Fofonoff (1996), Oceanic heat flux calculation, *J. Atmos. Ocean. Technol.*, *13*, 1327–1329.

Batchelor, G. K. (1967), *An Introduction to Fluid Dynamics*, Cambridge University Press, Cambridge, England.

Bleck, R. (2002), An oceanic general circulation model framed in hybrid isopycnic-Cartesian coordinates, *Ocean Model.*, *4*, 55–88.

Bleck, R., and D. B. Boudra (1981), Initial testing of a numerical ocean circulation model using a hybrid- (quasi-isopycnic) vertical coordinate, *J. Phys. Oceanogr.*, *11*, 755–770.

Bleck, R., and L. Smith (1990), A wind-driven isopycnic coordinate model of the north and equatorial Atlantic Ocean. 1. Model development and supporting experiments, *J. Geophys. Res.*, *95*(C3), 3273–3285.

Bleck, R., C. Rooth, D. Hu, and L. T. Smith (1992), Salinity-driven thermocline transients in a wind and thermohaline forced isopycnic coordinate model of the North Atlantic, *J. Phys. Oceanogr.*, *22*, 1486–1505.

Blumberg, A. F., and G. L. Mellor (1987), A description of a three-dimensional coastal ocean circulation model, in *Three-Dimensional Coastal Ocean Models, Coastal and Estuarine Series,* vol. 4, edited by N. Heaps, AGU, Washington, DC.

Bokhove, O. (2000), On hydrostatic flows in isentropic coordinates, *J. Fluid Mech.*, *402*, 291–310.

Browning, G., W. Holland, H. Kreiss, and S. Worley (1990), An accurate hyperbolic system for approximately hydrostatic and incompressible oceanographic flows, *Dyn. Atmos. Oceans*, *14*, 303–332.

Bryan, K. (1969a), A numerical method for the study of the circulation of the world ocean, *J. Comput. Phys.*, *4*, 347–376.

Bryan, K. (1969b), Climate and the ocean circulation III: The ocean model, *Mon. Weather Rev.*, *97*, 806–824.

Bryan, K., and M. D. Cox (1967), A numerical investigation of the oceanic general circulation, *Tellus*, *XIX*, 54–80.

Bryan, K., and M. D. Cox (1972), An approximate equation of state for numerical models of the ocean circulation, *J. Phys. Oceanogr.*, *4*, 510–514.

Bryan, K., and L. Lewis (1979), A water mass model of the world ocean, *J. Geophys. Res.*, *84*(C5), 2503–2517.

Bryan, K., S. Manabe, and R. C. Pacanowski (1975), A global ocean atmosphere climate model. Part II. The oceanic circulation, *J. Phys. Oceanogr.*, *5*, 30–46.

Campin, J.-M., A. Adcroft, C. Hill, and J. Marshall (2004), Conservation of properties in a free-surface model, *Ocean Model.*, *6*, 221–244.

Chaikin, P. M., and T. C. Lubensky (1995), *Principles of Condensed Matter Physics*, Cambridge University Press, Cambridge, United Kingdom.

Chassignet, E. P., and Z. Garraffo (2001), Viscosity parameterization and the Gulf Stream separation, in *From Stirring to Mixing in a Stratified Ocean*, edited by P. Müller and D. Henderson, Proceedings of the 12th 'Aha Huliko'a Hawaiian Winter Workshop, pp. 37–41, University of Hawaii at Manoa.

Chorin, A. (1968), Numerical solution of the Navier–Stokes equations, *Mathematical Computations*, 22, 745–762.

Cox, M. D. (1984), *A Primitive Equation, 3-Dimensional Model of the Ocean*, NOAA/Geophysical Fluid Dynamics Laboratory, Princeton, USA.

Cushman-Roisin, B. (1994), *Introduction to Geophysical Fluid Dynamics*, Prentice-Hall, Englewood Cliffs, USA, 320 + xv pp.

Davis, R. E. (1994), Diapycnal mixing in the ocean: equations for large-scale budgets, *J. Phys. Oceanogr.*, *24*, 777–800.

DeGroot, S. R., and P. Mazur (1984), *Non-Equilibrium Thermodynamics*, Dover Publications, New York, 510.

DeSzoeke, R. A., and R. M. Samelson (2002), The duality between the Boussinesq and non-Boussinesq hydrostatic equations of motion, *J. Phys. Oceanogr.*, *32*, 2194–2203.

Dewar, W. K., Y. Hsueh, T. J. McDougall, and D. Yuan (1998), Calculation of pressure in ocean simulations, *J. Phys. Oceanogr.*, *28*, 577–588.

Dukowicz, J., and R. Smith (1994), Implicit free-surface method for the Bryan–Cox–Semtner ocean model, *J. Geophys. Res.*, *99*(C4), 7991–8014.

Durran, D. R. (1999), *Numerical Methods for Wave Equations in Geophysical Fluid Dynamics*, Springer, Berlin, 470 pp.

Ertel, H. (1942), Ein neuer hydrodynamicscher wirbelsatz, *Meteorol. Z.*, *59*, 271–281.

Feistel, R. (1993), Equilibrium thermodynamics of seawater revisited, *Progr. Oceanogr.*, *31*, 101–179.

Feistel, R. (2003), A new extended Gibbs thermodynamic potential of seawater, *Progr. Oceanogr.*, *58*, 43–114.

Feistel, R., and E. Hagen (1995), On the Gibbs thermodynamic potential of seawater, *Progr. Oceanogr.*, *36*, 249–327.

Fofonoff, N. P. (1962), Physical properties of seawater, in *The Sea*, vol. 1, edited by M. N. Hill, pp. 3–30, Wiley-Interscience, New York.

Fox-Rabinovitz, M. (1991), Computational dispersion of horizontal staggered grids for atmospheric and ocean models, *Mon. Weather Rev.*, *119*, 1624–1639.

Gent, P. R., and J. C. McWilliams (1990), Isopycnal mixing in ocean circulation models, *J. Phys. Oceanogr.*, *20*, 150–155.

Gent, P. R., J. Willebrand, T. J. McDougall, and J. C. McWilliams (1995), Parameterizing eddy-induced tracer transports in ocean circulation models, *J. Phys. Oceanogr.*, *25*, 463–474.

Gill, A. (1982), *Atmosphere-Ocean Dynamics, International Geophysics Series*, vol. 30, Academic, London, 662 + xv pp.

Greatbatch, R. J. (1994), A note on the representation of steric sea level in models that conserve volume rather than mass, *J. Geophys. Res.*, *99*(C6), 12,767–12,771.

Greatbatch, R. J., Y. Lu, and Y. Cai (2001), Relaxing the Boussinesq approximation in ocean circulation models, *J. Atmos. Ocean. Technol.*, *18*, 1911–1923.

Gregg, M., T. Sanford, and D. Winkel (2003), Reduced mixing from the breaking of internal waves in equatorial waters, *Nature*, *422*, 513–515.

Gregg, M. C. (1984), Entropy generation in the ocean by small-scale mixing, *J. Phys. Oceanogr.*, *14*, 688–711.

Gregg, M. (1987), Diapycnal mixing in the thermocline: A review, *J. Geophys. Res.*, *92*(C5), 5249–5286.

Griffies, S. M. (2004), *Fundamentals of Ocean Climate Models*, Princeton University Press, Princeton, USA, 518 + xxxiv pages.

Griffies, S. M. (2005), Some ocean model fundamentals, in *Ocean Weather Forecasting: an Integrated View of Oceanography*, vol. 577, edited by E. P. Chassignet, and J. Verron, pp. 19–73, Springer, Berlin.

Griffies, S. M. (2007), *Elements of mom4p1*, NOAA/Geophysical Fluid Dynamics Laboratory, Princeton, USA, 346 pp.

Griffies, S. M., and R. W. Hallberg (2000), Biharmonic friction with a Smagorinsky viscosity for use in large-scale eddy-permitting ocean models, *Mon. Weather Rev.*, *128*, 2935–2946.

Griffies, S. M., C. Böning, F. O. Bryan, E. P. Chassignet, R. Gerdes, H. Hasumi, A. Hirst, A.-M. Treguier, and D. Webb (2000a), Developments in ocean climate modelling, *Ocean Model.*, *2*, 123–192.

Griffies, S. M., R. C. Pacanowski, and R. W. Hallberg (2000b), Spurious diapycnal mixing associated with advection in a *z*-coordinate ocean model, *Mon. Weather Rev.*, *128*, 538–564.

Griffies, S. M., R. Pacanowski, M. Schmidt, and V. Balaji (2001), Tracer conservation with an explicit free surface method for *z*-coordinate ocean models, *Mon. Weather Rev.*, *129*, 1081–1098.

Griffies, S. M., M. J. Harrison, R. C. Pacanowski, and A. Rosati (2004), *A Technical Guide to MOM4*, NOAA/Geophysical Fluid Dynamics Laboratory, Princeton, USA, 337 pp.

Haidvogel, D. B., and A. Beckmann (1999), *Numerical Ocean Circulation Modeling*, Imperial College Press, London.

Hallberg, R. W. (1997), Stable split time stepping schemes for large-scale ocean modeling, *J. Comput. Phys.*, *135*, 54–65.

Hallberg, R. W. (2000), Time integration of diapycnal diffusion and Richardson number-dependent mixing in isopycnal coordinate ocean models., *Mon. Weather Rev.*, *128*, 1402–1419.

Haltiner, G. T., and R. T. Williams (1980), *Numerical Prediction and Dynamic Meteorology*, Wiley, New York, USA.

Higdon, R. (2005), A two-level time-stepping method for layered ocean circulation models: further development and testing, *J. Comput. Phys.*, *206*, 463–504.

Higdon, R. (2006), Numerical modelling of ocean circulation, *Acta Numer.*, pp. 385–470.

Hirsch, C. (1988), *Numerical Computation of Internal and External Flows*, Wiley, New York.

Hirt, C., A. Amsden, and J. Cook (1974), An arbitrary Lagrangian–Eulerian computing method for all flow speeds, *J. Comput. Phys.*, *14*, 227–253.

Holloway, G. (1992), Representing topographic stress for large-scale ocean models, *J. Phys. Oceanogr.*, *22*, 1033–1046.

Huang, R. X. (1993), Real freshwater flux as a natural boundary condition for the salinity balance and thermohaline circulation forced by evaporation and precipitation, *J. Phys. Oceanogr.*, *23*, 2428–2446.

Huang, R. X., X. Jin, and X. Zhang (2001), An oceanic general circulation model in pressure coordinates, *Advances in Atmospheric Physics*, *18*, 1–22.

Jackett, D. R., T. J. McDougall, R. Feistel, D. G. Wright, and S. M. Griffies (2006), Algorithms for density, potential temperature, conservative temperature, and freezing temperature of seawater, *J. Atmos. Ocean. Technol.*, *23*, 1709–1728.

Killworth, P. (1989), On the parameterisation of deep convection in ocean models, in *Parameterizing Small Scale Processes in the Ocean*, edited by P. Müller and G. Holloway, Proceeding of the 5th 'Aha Huliko'a Hawaiian Winter Workshop, pp. 59–74, University of Hawaii at Manoa.

Killworth, P. D., D. Stainforth, D. J. Webb, and S. M. Paterson (1991), The development of a free-surface Bryan-Cox-Semtner ocean model, *J. Phys. Oceanogr.*, *21*, 1333–1348.

Landau, L. D., and E. M. Lifshitz (1987), *Fluid Mechanics*, Pergamon Press, Oxford, UK, 539 pp.

Large, W. G., G. Danabasoglu, J. C. McWilliams, P. R. Gent, and F. O. Bryan (2001), Equatorial circulation of a global ocean climate model with anisotropic horizontal viscosity, *J. Phys. Oceanogr.*, *31*, 518–536.

Ledwell, J. R., A. J. Watson, and C. S. Law (1993), Evidence for slow mixing across the pycnocline from an open-ocean tracer-release experiment, *Nature*, *364*, 701–703.

Lin, S. J. (1997), A finite volume integration method for computing pressure gradient force in general vertical coordinates, *Q. J. R. Meteorol. Soc.*, *123*, 1749–1762.

Lion, J., R. Temam, and S. Wang (1992), On the equations of the largescale ocean, *Nonlinearity*, *5*, 1007–1053.

Losch, M., A. Adcroft, and J.-M. Campin (2004), How sensitive are coarse general circulation models to fundamental approximations in the equations of motion?, *J. Phys. Oceanogr.*, *34*, 306–319.

Margolin, L., W. Rider, and F. Grinstein (2006), Modeling turbulent flow with implicit LES, *J. Turbul.*, *7*, 1–27.

Marion, J. B., and S. T. Thornton (1988), *Classical Dynamics of Particles and Systems*, Harcourt Brace Jovanovich, San Diego, USA, 602 pp.

Marshall, J., and F. Schott (1999), Open-ocean convection: observations, theory, and models, *Rev. Geophys.*, *37*, 1–64.

Marshall, J., C. Hill, L. Perelman, and A. Adcroft (1997), Hydrostatic, quasi-hydrostatic, and nonhydrostatic ocean modeling, *J. Geophys. Res.*, *102*(C3), 5733–5752.

Marshall, J., A. Adcroft, J.-M. Campin, and C. Hill (2004), Atmosphere–ocean modeling exploiting fluid isomorphisms, *Mon. Weather Rev.*, *132*, 2882–2894.

McDougall, T., and W. Dewar (1997), Vertical mixing and cabbeling in layered models, *J. Phys. Oceanogr.*, *28*, 1458–1480.

McDougall, T. J. (1987), Neutral surfaces, *J. Phys. Oceanogr.*, *17*, 1950–1967.

McDougall, T. J. (2003), Potential enthalpy: A conservative oceanic variable for evaluating heat content and heat fluxes., *J. Phys. Oceanogr.*, *33*, 945–963.

McDougall, T. J., R. J. Greatbatch, and Y. Lu (2003), On conservation equations in oceanography: How accurate are Boussinesq ocean models?, *J. Phys. Oceanogr.*, *32*, 1574–1584.

Mellor, G. L., and T. Ezer (1995), Sea level variations induced by heating and cooling: an evaluation of the Boussinesq approximation in ocean models, *J. Geophys. Res.*, *100*(C10), 20,565–20,577.

Mesinger, F. (1973), A method for construction of second-order accurate difference schemes permitting no false two-grid-interval waves in the height field., *Tellus*, *25*, 444–457.

Mesinger, F., and A. Arakawa (1976), Numerical methods used in atmospheric models, in *GARP Publication Series*, vol. 1, p. 66 pages.

Morse, P. M., and H. Feshbach (1953), *Methods of Theoretical Physics Part I and II*, McGraw-Hill Book Company, New York.

Müller, P. (1995), Ertel's potential vorticity theorem in physical oceanography, *Rev. Geophys.*, *33*, 67–97.

Müller, P. (2006), *The Equations of Oceanic Motions*, 1st ed., Cambridge University Press, Cambridge, 302 pp.

Müller and J. Willebrand, P. (1986), Compressibility effects in the thermohaline circulation: A manifestation of the temperature salinity mode, *Deep Sea Res.*, *33*, 559–571.

Munk, W. H. (1950), On the wind-driven ocean circulation, *Journal of Meteorology*, *7*, 79–93.

Oberhuber, J. (1993), Simulation of the atlantic circulation with a coupled sea ice-mixed layer-isopycnal general circulation model. Part I: Model description, *J. Phys. Oceanogr.*, *23*, 808–829.

Osborn, T. R. (1980), Estimates of the local rate of vertical diffusion from dissipation measurements, *J. Phys. Oceanogr.*, *10*, 83–89.

Pedlosky, J. (1987), *Geophysical Fluid Dynamics*, 2nd ed., Springer, Berlin, 710 + xv pp.

Phillips, N. (1973), Principles of large-scale numerical weather prediction, in *Dynamic Meteorology*, edited by P. Morel, pp. 1–96, Riedel, Boston.

Phillips, N. A. (1957), A coordinate system having some special advantages for numerical forecasting, *J. Meteorol.*, *14*, 184–185.

Roberts, M. J., and D. Marshall (1998), Do we require adiabatic dissipation schemes in eddy-resolving ocean models?, *J. Phys. Oceanogr.*, *28*, 2050–2063.

Rosati, A., and K. Miyakoda (1988), A general circulation model for upper ocean simulation, *J. Phys. Oceanogr.*, *18*, 1601–1626.

Russell, G. L., J. R. Miller, and D. Rind (1995), A coupled atmosphere ocean model for transient climate change studies, *Atmosphere-Ocean*, *33*, 683–730.

Sadourny, R. (1975), The dynamics of finite-difference models of the shallow-water equations, *J. Atmos. Sci.*, *32*, 680–689.

Salmon, R. (1998), *Lectures on Geophysical Fluid Dynamics*, Oxford University Press, Oxford, England, 378 + xiii pp.

Semtner, A. J., and Y. Mintz (1977), Numerical simulation of the Gulf Stream and mid-ocean eddies, *J. Phys. Oceanogr.*, *7*, 208–230.

Smagorinsky, J. (1963), General circulation experiments with the primitive equations: I. The basic experiment, *Mon. Weather Rev.*, *91*, 99–164.

Smagorinsky, J. (1993), Some historical remarks on the use of nonlinear viscosities, in *Large Eddy Simulation of Complex Engineering and Geophysical Flows*, edited by B. Galperin and S. A. Orszag, pp. 3–36, Cambridge University Press, Cambridge.

Smith, R. D., and P. R. Gent (2004), Anisotropic Gent–McWilliams parameterization for ocean models, *J. Phys. Oceanogr.*, *34*, 2541–2564.

Smith, R. D., and J. C. McWilliams (2003), Anisotropic horizontal viscosity for ocean models, *Ocean Model.*, *5*, 129–156.

Vallis, G. K. (2006), *Atmospheric and Oceanic Fluid Dynamics: Fundamentals and Large-scale Circulation*, 1st ed., Cambridge University Press, Cambridge, 745 + xxv pp.

Veronis, G. (1973), Large scale ocean circulation, *Adv. Appl. Mech.*, *13*, 2–92.

Wajsowicz, R. C. (1986), Adjustment of the ocean under buoyancy forces. Part II: The role of planetary waves, *J. Phys. Oceanogr.*, *32*, 2115–2136.

White, L., V. Legat, and E. Deleersnijder (2008), Tracer conservation for three-dimensional, finite element, free-surface, ocean modeling on moving prismatic meshes, *Mon. Weather Rev.*, (in press), doi: 10.1175/2007MWR2137.1.

Stephen M. Griffies, NOAA Geophysical Fluid Dynamics Laboratory, Princeton Forrestal Campus Rte. 1, 201 Forrestal Road, Princeton, NJ 08542, USA. (Stephen.Griffies@noaa.gov)